Midinfrared spectroscopy of synthetic olivines: Thermal emission, specular and diffuse reflectance, and attenuated total reflectance studies of forsterite to fayalite

Melissa D. Lane,[1] Timothy D. Glotch,[2] M. Darby Dyar,[3] Carle M. Pieters,[4] Rachel Klima,[5] Takahiro Hiroi,[4] Janice L. Bishop,[6] and Jessica Sunshine[7]

Received 24 February 2010; revised 12 May 2011; accepted 27 May 2011; published 27 August 2011.

[1] Synthetic olivine samples ranging in composition from forsterite to fayalite are analyzed in the midinfrared using thermal emission, specular and diffuse reflectance, and attenuated total reflectance spectroscopies to study the spectral effects of Mg-Fe solid solution. For each method, fundamental bands gradually change in position and strength from Mg_2SiO_4 at larger wave numbers to Fe_2SiO_4 at smaller wave numbers. Each spectrum is diagnostic of chemistry within the continuum, as previously noted. In this study, 10 identified fundamental bands are traceable across the solid solution series for each technique. In pelletized sample spectra, the 10 bands shift approximately linearly in position by as little as 11 to as much as 64 cm^{-1}. In powdered sample spectra, the bands shift by as little as 12 to as much as 74 cm^{-1} (disregarding one outlier point). Moreover, for *every* spectral technique, an even larger linear shift is identified of a specific emissivity maximum/reflectivity minimum (the flection position). From forsterite to fayalite, this flection position shifts by at least 88 cm^{-1}, which is, on average, *48% more* than the largest fundamental band shift within the same data set for the pelletized spectra and *44% more* for the powdered spectra. Also the R^2 and 2σ values of the best fit line for the flection position shift (versus $Fo_{\#}$) generally were as good as or routinely better than those of the fundamental bands. Thus, the flection position should be considered as a means of determining Mg-Fe olivine composition when using thermal emission, specular reflectance, diffuse reflectance, or attenuated total reflectance spectroscopic data.

Citation: Lane, M. D., T. D. Glotch, M. D. Dyar, C. M. Pieters, R. Klima, T. Hiroi, J. L. Bishop, and J. Sunshine (2011), Midinfrared spectroscopy of synthetic olivines: Thermal emission, specular and diffuse reflectance, and attenuated total reflectance studies of forsterite to fayalite, *J. Geophys. Res.*, *116*, E08010, doi:10.1029/2010JE003588.

1. Introduction

[2] Olivine minerals are some of the most abundant minerals in the solar system and their chemistry is variable, as is the chemistry of many naturally occurring minerals. Common rock-forming olivines range in composition from the Mg-bearing forsterite species ([Fo_{100}], Mg_2SiO_4) to Fe-bearing fayalite ([Fo_0], Fe_2SiO_4), and substitution of those two cations occurs in this common binary solid solution series (i.e., $(Mg_X, Fe_{1-x})_2SiO_4$ ($0 \leq \times \leq 1$)). Generally, the structure of ferromagnesian olivine can be described as an arrangement of isolated silica tetrahedra, alternately pointing in opposite directions along the *a* axis. Among these silica tetrahedra are the metal cations (e.g., M = Mg, Fe) in interstitial rows of either M1 or M2 octahedral sites at different levels along the *c* axis. Both tetrahedral and octahedral sites are slightly distorted from an ideal shape; hence, degeneracies are removed and additional features arise in the midinfrared (vibrational) spectra. Accordingly, changes in chemistry across this binary series cause the structure of the mineral to be affected, in turn influencing the internal vibrations of the constituent molecules and the external lattice vibrations as represented in their midinfrared spectra.

[3] The midinfrared spectral behavior of *natural* olivine (commonly contaminated by Mn^{2+} or other divalent cations) has been studied by numerous researchers prior to this work [e.g., *Lehmann et al.*, 1961; *Duke and Stephens*, 1964; *Burns*

[1]Planetary Science Institute, Tucson, Arizona, USA.
[2]Department of Geosciences, State University of New York at Stony Brook, Stony Brook, New York, USA.
[3]Department of Astronomy and Geology, Mount Holyoke College, South Hadley, Massachusetts, USA.
[4]Department of Geological Sciences, Brown University, Providence, Rhode Island, USA.
[5]Space Department, Johns Hopkins University Applied Physics Laboratory, Laurel, Maryland, USA.
[6]SETI Institute and NASA Ames Research Center, Mountain View, California, USA.
[7]Department of Astronomy, University of Maryland, College Park, Maryland, USA.

0148-0227/11/2010JE003588

and Huggins, 1972; *Runciman et al.* 1973; *Salisbury et al.*, 1991b; *Tarantino et al.*, 2003; *Koeppen and Hamilton*, 2008; *Hamilton*, 2010]; however, this work introduces a large Mg-Fe suite of *synthetic* olivine samples. Although some synthetic olivine spectra have been published before in transmission [e.g., *Tarantino et al.*, 2003; *Koike et al.*, 2003; *Hofmeister and Pitman*, 2007; *Pitman et al.*, 2010] and reflectance [*Sogawa et al.*, 2006], this work represents the first time *emissivity* and *attenuated total reflectivity* spectra of a full Mg-Fe *synthetic*-olivine suite have been published, and extends the spectral range for *reflectance* data acquired of more numerous chemical subdivisions than most previous (dominantly transmission) works (with the exception of *Hofmeister and Pitman* [2007] and *Koike et al.* [2003]), and presents the spectra of a single set of synthesized samples both analyzed and cross-compared using an unprecedented four different midinfrared spectroscopic techniques.

[4] This paper is one of a series of papers that present the spectroscopic characteristics of a single suite of synthesized (pure) olivine samples in order to interrelate the spectral features identified using various spectroscopic instruments and create a multitechnique set of reference spectra of the forsterite-fayalite solid solution series. In the first paper of this group, *Dyar et al.* [2009] discussed in detail the experimental methods used to synthesize the olivine solid solution samples and verified the compositions of the well-characterized olivines by X-ray diffraction and by diverse analytical spectroscopic techniques including Mössbauer, Raman, thermal (mid-) infrared emission, midinfrared attenuated total reflectance and specular reflectance, and visible-near infrared (VNIR) to midinfrared diffuse reflectance spectroscopies. *Dyar et al.* [2009] presented only the spectrum of fayalite (Fo_0) for each technique listed above as an example of the utility of combined multitechnique spectroscopic analyses. The exception was for the 295 K Mössbauer results that were presented for the entire Mg-Fe olivine suite to inform the discussion of Fe^{3+} and sample purity.

[5] In this study we present olivine spectra from synthetic forsterite to fayalite that were measured in the midinfrared range of the electromagnetic spectrum by several techniques including thermal emission, specular reflectance, diffuse reflectance, and attenuated total reflectance spectroscopies. In this study we identify and discuss the spectral variation over a broad range of Mg-Fe solid solution chemistries of olivine. The olivine spectra generated from this work can be used for comparison with other spectra in order to determine specific olivine compositions in hand sample spectra (of rocks, sediments, or meteorites) and remote sensing spectra (including in situ attenuated total reflectivity) of Earth and other planetary surfaces, as well as of asteroids, dead comets (i.e., rocky comets whose icy components have been eroded away over time), or spectra associated with stars. Application of emissivity and reflectivity spectra of natural olivines to remote sensing data for the determination of the presence of and compositions of olivine have been conducted previously [e.g., *Pieters*, 1982; *Cruikshank and Hartmann*, 1984; *Gaffey et al.*, 1993a; *Lucey et al.*, 1998; *Christensen et al.*, 2000a; *Hoefen et al.*, 2003; *Hamilton and Christensen*, 2005; *McSween et al.*, 2006; *Ruff et al.*, 2006; *Poulet et al.*, 2007; *Rogers and Christensen*, 2007; *Sunshine et al.*, 2007; *Koeppen and Hamilton*, 2008; *Edwards et al.*, 2008; *Bandfield and Rogers*, 2008]; also, the specific synthetic olivine spectra presented here have been applied with success to the identification of olivine and its composition in meteorites and Martian remote sensing data to a limited degree [e.g., *Lane et al.*, 2009; *Dyar et al.*, 2011; *Lane and Goodrich*, 2010].

[6] Here we discuss in detail the acquisition of laboratory spectra of a synthetic Mg-Fe olivine suite and the spectral variation that occurs per spectral technique as related to the sample chemistry. Historically, the use of fundamental band positions for compositional analysis has been presented and here we also discuss the shifting of band positions as they apply to our synthetic olivine spectra. Furthermore, we introduce the systematic behavior of a farther shifting interband feature (i.e., a spectral region located between two fundamental bands that we call a flection position because it is a local emissivity maximum/reflectivity minimum) and discuss its utility for identifying olivine composition. We also present data in support of a linear relationship between composition and transparency band width for powdered samples measured in diffuse reflectance.

2. Sample Description

[7] Olivine samples used for this study were the same as those presented by *Dyar et al.* [2009]; however, this study presents and discusses only the olivines synthesized by Donald Lindsley at Stony Brook University (i.e., "SUNY olivines") and excludes the "Bristol olivines" because of their impurities. The Lindsley synthesis experiments were designed to ensure that the chemistries would stay the proper composition during their production. All starting materials were dried properly by using tested procedures, errors in weighing of reagents were avoided (weighing errors would be detected because additional phases would appear in the reacted material), oxidation was prevented (as confirmed by Mössbauer spectroscopy), and incomplete reactions were avoided by repeatedly grinding and reheating samples until the products were single-phase (confirmed by X-ray diffraction). With the electron microprobe, several samples were spot checked to rule out the possibility that the single-phase olivines were zoned and thus chemically heterogeneous; no zoned samples were found, and all were the exact proper composition. We are confident that the samples truly represent their stated compositions. For additional discussion regarding the sample synthesis technique and their compositions, see *Dyar et al.* [2009]. The samples vary in composition from forsterite (Fo_{100}) to fayalite (Fo_0) and include the intermediate compositions $Fo_{89.5}$, Fo_{80}, Fo_{75}, Fo_{70}, Fo_{65}, Fo_{60}, Fo_{55}, Fo_{50}, Fo_{40}, Fo_{30}, Fo_{20}, and Fo_{10}.

[8] For this study the synthesized finely powdered (<45 μm) olivine samples were made into small (~5–10 mm diameter) compact pellets using a standard Carver hydraulic 13 mm press and die. Pure mineral powders were pressed for ~2 min at 18,000 psi. Some of the edges of these pellets chipped away, and some of them cracked into several smaller pieces, making the samples smaller than their original size. These pellets, which represent many crystal orientations, were analyzed by thermal emission, specular reflectance, and diffuse reflectance, and the synthetic olivine samples as loose powders

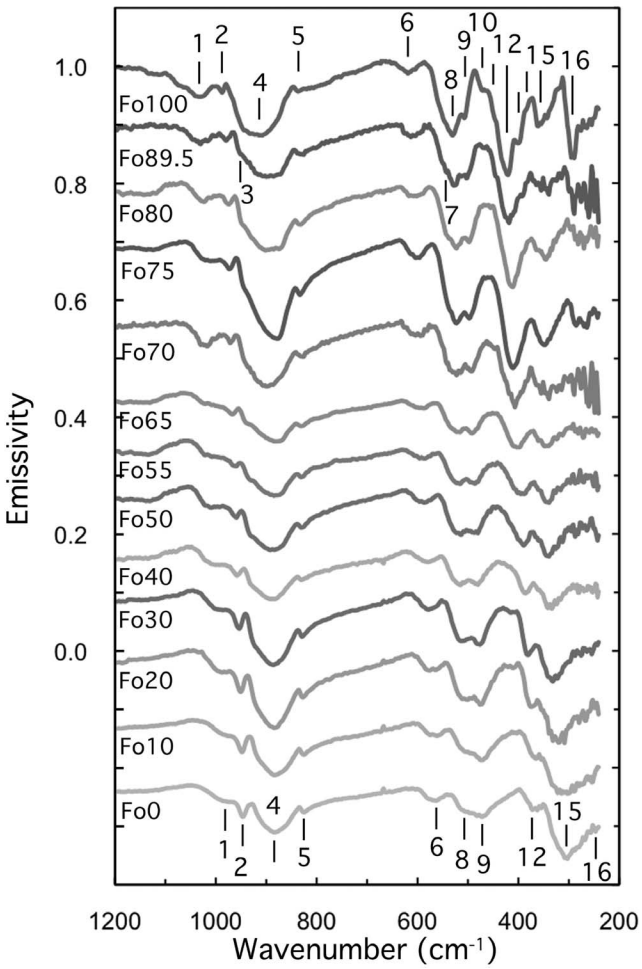

Figure 1. Thermal emissivity spectra of the pressed pellets made from synthetic Mg-Fe olivines across the solid solution series. Spectra are offset for clarity. Some water vapor that was not removed fully by the calibration method appears as noise (jaggedness) in the spectra at long wavelengths. Band numbers are noted.

were analyzed with diffuse reflectance and attenuated total reflectance spectroscopies.

3. Midinfrared Spectroscopic Methods

3.1. Thermal Emission

[9] Thermal emissivity spectra were acquired at the Arizona State University (ASU) Mars Space Flight Facility. The ASU laboratory hosts a Nicolet Nexus 670 FTIR interferometric spectrometer that has been modified for emission measurements by removal of the SiC source and placement of an enclosed glove box and folding mirrors outside the spectrometer housing to enable the energy from a heated sample in a sample chamber within the glove box to enter into the raypath for measurement. The chamber is water-cooled to maintain the environmental temperature. The atmosphere is scrubbed of CO_2 and H_2O to eliminate those spectral lines from the sample data. The spectrometer is equipped with a thermoelectrically stabilized deuterated triglycine sulfate (DTGS) detector and a CsI beam splitter that allows quality measurement of emitted radiation over the midinfrared range of 2000 to 240 cm^{-1} (5 to 42 μm) [e.g., *Ruff et al.*, 1997].

[10] For each measurement, the olivine pellet was placed in a copper sample cup, painted with Aeroglaze® Z302 gloss black paint, and heated to and maintained at an 80°C set point for the duration of the measurements. The 160 scans of each sample were acquired at ~4 cm^{-1} spectral resolution (~2 cm^{-1} spectral sampling) and the individual scan spectra were averaged together. This resulting sample radiance spectrum was calibrated according to the procedure discussed in detail by *Ruff et al.* [1997] and converted to spectral emissivity. No additional spectral filtering was performed.

[11] The Fo_{60} pellet sample was too small to be measured by the thermal emission technique, so it is not discussed in further detail regarding sample emissivity. Eleven of the remaining 13 samples were very small (<5 mm diameter) and the spot size of the spectrometer (>~1 cm diameter) was larger than the samples; therefore, it was necessary to subtract a large fraction of the emissivity spectrum of an empty sample cup (a blank) from the calibrated emissivity spectrum of these samples to return a representative mineral spectrum. Two samples (Fo_{70} and $Fo_{89.5}$) were larger in diameter (~1 cm; synthesized and pelletized later) and required less sample cup emissivity correction. For all 13 usable samples, thermal emissivity spectra of sufficient quality were acquired (Figure 1). Spectral band positions (Table 1) were determined by locating the wave number value of each local band emissivity minimum. The emissivity spectra are available at http://speclib.asu.edu.

3.2. Specular Reflectance

[12] Specular reflectivity spectra (from 4000 to 100 cm^{-1}; 2.5 to 100 μm) of the pellets (minus the too-small Fo_{60} sample) were acquired at state University of New York at Stony Brook using a Nicolet FT-30 specular reflectance accessory with incidence and reflection angles of 30°. These 4 cm^{-1} resolution (2 cm^{-1} sampling) spectra were acquired in two parts: from 4000 to 400 cm^{-1} using an uncooled DLaTGS detector with a KBr window and a KBr beam splitter and from 600 to 200 cm^{-1} using a Nicolet Solid Substrate beam splitter and a DTGS detector with a polyethylene window. Several corrections were applied in order to splice the spectra. First, the "reflectance function" of the reflectance accessory and the standard were characterized by acquiring a background spectrum without the accessory in the spectrometer. The accessory was then inserted into the spectrometer with the reflectance standard, and a spectrum was collected. This spectrum represented the combined reflectance of the mirrors in the reflectance accessory and the reflectance standard. Because the olivine pellets are small compared with the size of the incident beam (~1 cm), this procedure accounts for the reflectance properties of the aperture mask on which the pellets sit. The bottom of the mask was coated with carbon black to reduce the reflectance of the mask as much as possible. Subsequent to the collection of the olivine pellet spectra, a spectrum of the "blank" aperture mask was acquired to characterize its reflectance. Both the olivine pellet and blank spectra were divided by the reflectance function spectrum. The blank spectrum was then subtracted from the pellet spectra.

Table 1. Thermal Emissivity Band Positions for the Forsterite-Fayalite Series[a]

	Band Number and Position in This Study ((cm^{-1})															
Sample	1 [1]	2 (1) [2]	3 (2)	4 (3) [3]	5 (4) [4]	6 (5) [5]	7 [5a]	8 (6) [6]	9 (7) [7]	10 [8]	11	12 [9]	13 [10]	14 [11]	15 [12]	16 [13]
Fo_{100}	1033	988		914	836	619		530	507	471	447 sh	420	401	383 sh	359	291
$Fo_{89.5}$	1031	980	951 w	900	832	613	542 w	527	503	468	445	419	393	372	347	286
Fo_{80}	1024	974	sh	902	833	607	538 w	523	498			411	389 sh	364	346	284[b]
Fo_{75}	1023	974	sh	879	833	600	536 sh	523	497			411			348	286
Fo_{70}	1017	972		899	829	594		523	493	446		407	382 sh	363 w	343	289[b]
Fo_{65}	1008	966	938 sh	882	831	588		519	492			400		360 w	345	272
Fo_{55}	1007	962	932 sh	885	831	586		515	486			395			342	286[b]
Fo_{50}	1009	959	930 sh	892	830	587		514	480	432 w	sh	389			340	284[b]
Fo_{40}	1000	959	sh	891	830	580		515	480	432 w		386		361 w	337	278 w
Fo_{30}	997	954	sh	886	829	578		513	477	415		381			332	278 w
Fo_{20}	988	951		884	828	576		501	476	411		375			320	
Fo_{10}	987	948		883	825	562		505 sh	473	403		365			315	254[b]
Fo_0	985	947		885	825	563		505 sh	472			363		sh	305	247[b] w
Δ_{band}	48	41		29	11	57		29	35			57			54	44
R^2	0.97	0.96		0.42	0.85	0.95		0.92	0.95			0.99			0.91	0.73
2σ	11.06	12.16		45.45	23.35	13.54		16.87	13.65			6.73			17.60	30.81

[a]Band assignments in parentheses are from *Duke and Stephens* [1964]; those in brackets are from *Hamilton* [2010] following *Burns and Huggins* [1972]; abbreviations are sh, shoulder; w, weak; Δ_{band}, maximum difference in band position (in wave number).
[b]Data are noisy, so position is uncertain.

[13] Mid- and far-IR spectra were spliced near 500 cm^{-1} to produce a single spectrum covering the range from 2000 to 100 cm^{-1} according to *Glotch et al.* [2007]. The pressing process used to make the small pellets (mentioned in section 2) produced flat surfaces from which single specular reflections are assumed in the mid- and far-IR spectral ranges [e.g., *Roush et al.*, 1991; *Glotch et al.*, 2004]. At wave numbers larger than ~2000 cm^{-1}, the assumption of a single specular reflection with no scattering becomes less valid, so specular reflectance analyses of pressed pellets were confined to the <2000 cm^{-1} region. For all 13 usable samples, specular reflectivity spectra of sufficient quality were acquired (Figure 2) to allow the band positions to be identified (Table 2). Spectral band positions were determined by locating the wave number value of each local band minimum. The specular reflectivity spectra are available at http://aram.ess.sunysb.edu/tglotch/spectra.html.edu.

3.3. Diffuse Reflectance

[14] Midinfrared diffuse reflectivity spectra were acquired for both pressed pellets and loose powders at the NASA/Keck Reflectance Experiment Laboratory (RELAB) at Brown University [*Pieters and Hiroi*, 2004] in a purged environment (CO_2- and H_2O-free) using a Pike diffuse reflectance accessory fit to a Thermo-Nicolet Nexus 870 Fourier transform infrared (FTIR) spectrometer with an off-axis biconical viewing geometry (30 ± 30 degrees in both incidence and emergence angles). Spectra were collected at 4 cm^{-1} resolution (2 cm^{-1} intervals) using a KBr beam splitter and DTGS detector (from ~7700 to 400 cm^{-1}; 1.3–25 μm) or a Nicolet Solid Substrate beam splitter and a DTGS detector with a polyethylene window (from 625 to 100 cm^{-1}; 16–100 μm). Instrument spot size is ~2 mm diameter. Raw spectra were ratioed to a diffuse gold reference standard and then scaled to the VNIR bidirectional spectra of these samples near 2.5 μm to provide absolute reflectance values. Only the mid-IR data are presented here; the VNIR reflectance data are not discussed in this paper.

[15] The Fo_{60} pellet sample fell apart and was too small to be measured using diffuse reflectance; however, that sample

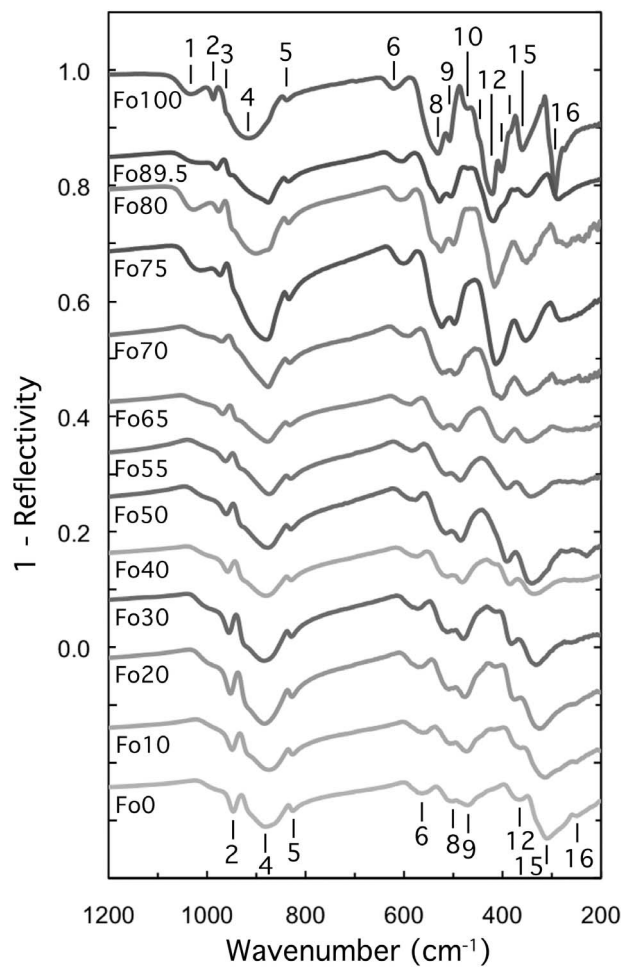

Figure 2. Specular reflectivity spectra of the pressed pellets made from synthetic Mg-Fe olivines across the solid solution series. Reflectivity values (R) may be compared with emissivity values (ε) according to Kirchhoff's Law ($\varepsilon = 1 - R$). Spectra are scaled to the emissivity data in Figure 1 and are offset for clarity. Band numbers are noted.

Table 2. Specular Reflectance Band Positions for the Forsterite-Fayalite Series[a]

	Band Number and Position in This Study (cm^{-1})															
Sample	1 [1]	2 (1) [2]	3 (2)	4 (3) [3]	5 (4) [4]	6 (5) [5]	7 [5a]	8 (6) [6]	9 (7) [7]	10 [8]	11	12 [9]	13 [10]	14 [11]	15 [12]	16 [13]
Fo_{100}	1034	988	961 w	914	838	621		531	507	471	448 sh	421	402	383	360	295
$Fo_{89.5}$	1030	981	953	876	835	605	sh	528	505	470		419	sh	375 w	351	287
Fo_{80}	1028	976	948	900	835	607	540 w	525	499			416			351	285[c] sh
Fo_{75}	1020	974	sh	880	834	601		523	498			414			353	282
Fo_{70}	sh	970		876	832	593		523	498			403			351	276[c]
Fo_{65}	sh	968	939 sh	877	833	587		519	492			397			351	279
Fo_{55}	sh	963	933 sh	874	830	584		515	486			392			344	277
Fo_{50}	sh	961	930 sh	875	829	577		514	485			391			341	271 w
Fo_{40}	sh	959	sh	879	829	574		512	482	416		384			337	
Fo_{30}	sh	956	sh	885	829	573		513	479	413		382			332	260 w
Fo_{20}	sh	953	sh	884	827	572		509	476	415		376			326	250 w
Fo_{10}	sh	949	sh	874	826	562		506	474	sh		364			315	251
Fo_0	sh	947		881	826	563		500	471			365		sh	310	248
Δ_{band}		41		40	12	59		31	36			57			50	47
R^{2b}	(0.84)	0.97		0.18	0.94	0.92		0.97	0.97			0.97			0.94	0.97
$2\sigma^b$	(7.56)	10.25		54.08	14.99	16.59		10.54	9.92			10.80			14.63	10.46

[a]Band assignments in parentheses are from *Duke and Stephens* [1964]; those in brackets are from *Hamilton* [2010] following *Burns and Huggins* [1972]; abbreviations are sh, shoulder; w, weak; Δ_{band}, maximum difference in band position (in wave number).
[b]Parentheses indicate R^2 and 2σ determined from only 4 points.
[c]Data are noisy, so position is uncertain.

was reground and measured in powdered form using the diffuse reflectance technique. This is the only technique presented in this work by which the Fo_{60} sample could be measured (and only in powdered form). For all 13 usable pellet samples, diffuse reflectivity spectra of sufficient quality were acquired (Figure 3) enabling the band positions to be identified (Table 3). The diffuse reflectivity spectra of the powders are shown in Figure 4, and their band positions are defined in Table 4 (including the Fo_{60} sample). Spectral band positions were determined by locating the wave number value of each local band minimum (as viewed in Figures 3 and 4). The diffuse reflectivity spectra are available at http://www.planetary.brown.edu/relab.

3.4. Attenuated Total Reflectance

[16] Attenuated total reflectance (ATR) data were acquired at Stony Brook University on a Nicolet 6700 FTIR spectrometer purged of CO_2 and H_2O and using the same detector and beam splitter combinations described for the specular reflectance measurements. The attenuated total reflectance accessory is a SmartOrbit ATR attachment with a type IIA diamond ATR element, with input and emergence angles of 45°. The measured spot size on the diamond element is ~1 mm. Spectra were collected at 4 cm^{-1} resolution between 1200 and 300 cm^{-1}. A total of 512 scans was averaged to create each spectrum. Attenuated total reflectivity spectra are referenced to a standard spectrum acquired without any sample on the diamond ATR element. This reference spectrum is the equivalent to the gold mirror background spectrum acquired for specular reflectance measurements.

[17] The Fo_{60} sample was too small to be measured by attenuated total reflectance because it broke into small pieces and some sample was lost, so the sample is not discussed further. The attenuated total reflectance spectra of the synthetic olivine powders are shown in Figure 5, and their band positions are defined in Table 5. Spectral band positions were determined by locating the wave number value of each local absorbance maximum. The attenuated total

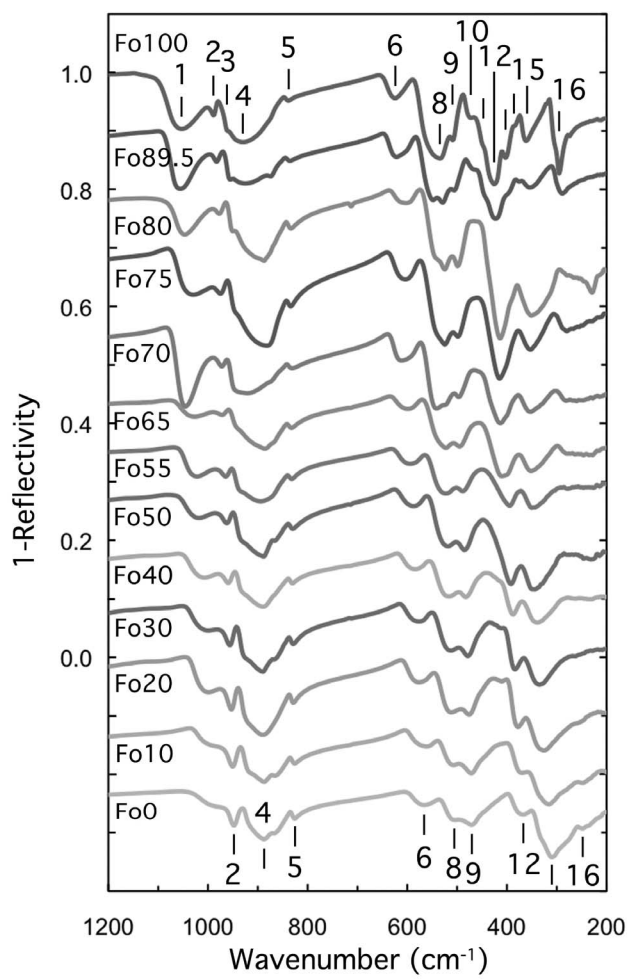

Figure 3. Diffuse reflectivity spectra of the pressed pellets made from synthetic Mg-Fe olivines across the solid solution series. Reflectivity values (R) may be compared with emissivity values (ε) according to Kirchhoff's Law ($\varepsilon = 1 - R$). Spectra are scaled to the emissivity data in Figure 1 and are offset for clarity. Band numbers are noted.

Table 3. Diffuse Reflectance Band Positions for the Forsterite-Fayalite Series[a]

	Band Number and Position in This Study (cm^{-1})															
Sample	1 (1)	2 (1) [2]	3 (2)	4 (3) [3]	5 (4) [4]	6 (5) [5]	7 [5a]	8 (6) [6]	9 (7) [7]	10 [8]	11	12 [9]	13 [10]	14 [11]	15 [12]	16 [13]
Fo_{100}	1053	989	961 w	930	838	625		535	509	473	449 sh	426	403	383 sh	361	295
$Fo_{89.5}$	1055	982	955	925	836	621	548	529	506	470	445 sh	423	394 sh	375 w	354	289
Fo_{80}	1047	978	950	887	834	604	542	525	499			413			351	279 sh
Fo_{75}	1030	975	sh	883	833	604		525	498			415			353	281
Fo_{70}	1046	972		921	831	611	541	524	497			413			353	279
Fo_{65}	1026	971		887	833	599		523	495			411			351	279 w
Fo_{55}	1022	964	sh	894	832	593		523	489			394			350	
Fo_{50}	1018	962	931 sh	888	830	588		518	486			391			345	
Fo_{40}	1007	959	sh	889	830	584		516	483	sh		388			339	
Fo_{30}	999	956	sh	890	829	577		512	478	411		384			335	264 w
Fo_{20}	999	953	sh	890	829	576		511	476	411		378			326	sh
Fo_{10}	1000	951	sh	887	826	561		507	472			369			316	248
Fo_0	sh	948		887	826	567		506	471			367		sh	310	249
Δ_{band}	56	41		43	12	64		29	38			59			51	47
R^2	0.91	0.97		0.37	0.92	0.95		0.98	0.99			0.97			0.92	0.97
2σ	16.36	10.05		47.58	16.77	13.33		9.52	7.18			9.95			16.25	11.08

[a]Band assignments in parentheses are from *Duke and Stephens* [1964]; those in brackets are from *Hamilton* [2010] following *Burns and Huggins* [1972]; abbreviations are sh, shoulder; w, weak; Δ_{band}, maximum difference in band position (in wave number).

reflectivity spectra are available at http://aram.ess.sunysb.edu/tglotch/spectra.html.

4. Results

4.1. Pressed Pellets: Thermal Emission

4.1.1. Fundamental Band Positions in Thermal Emissivity Spectra

[18] Systematic changes in chemistry and structure of the synthesized ferromagnesian olivines enable the systematic variations of the spectral bands to be studied. Thermal emissivity spectra of all of the olivine samples are shown in Figure 1. Over the spectral range, the Mg-Fe olivine suite exhibits 16 distinct bands, some of which are subtle or are not apparent across the entire solid solution series (Table 1). The forsterite spectrum exhibits 14 total bands (of which two occur as shoulders). The fayalite spectrum shows fewer bands overall than the forsterite (i.e., 11 total bands, of which one is a shoulder), and they are all shifted to lower frequency (smaller wave numbers) than the same bands in the Mg-rich olivine (Table 1). As shown in Figure 1, spectra from all of the intermediate compositions grade between the Mg- and the Fe-olivine end-member spectra and show progressive displacement of the bands toward longer wavelengths (smaller wave numbers) with increasing Fe content (decreasing $Fo_{\#}$).

[19] It was difficult to specify the emissivity minimum for some bands because they are either very broad and/or occur as shoulders on stronger bands (with an uncertainty in position of ±6 cm^{-1}). Because these samples are pressed powders, the bands present likely could be representative of more than one single-crystal vibrational mode [*Hofmeister*, 1987], although some probably do represent a single mode. For the sake of the following discussion, the spectral features for fayalite and forsterite are labeled by band number (band 1, band 2, etc.) (These values do not correspond exactly to the similar band-numbering system of *Burns and Huggins* [1972] adopted by *Hamilton* [2010] or of *Duke and Stephens* [1964], but those band names are shown in Tables 1–5 for comparison with our band numbering system.)

[20] In forsterite, bands are seen that are not present in fayalite. However, 10 spectral features are clear and traceable across the Mg-Fe olivine series compositions (Table 1) and include bands 1, 2, 4, 5, 6, 8, 9, 12, 15, and 16. Bands 1, 2, and 4 result from the asymmetric Si-O stretching vibrations (ν_3); the symmetric stretching vibration (ν_1) appears as band 5; longer-wavelength bands 6, 8, and 9 result from the ν_4 in-plane bending modes. The remaining bands 12, 15, and 16 are due to translations and (hindered) rotations of the SiO_4 tetrahedra and translations of the metal in the structure [e.g., *Iishi*, 1978; *Bowey et al.*, 2001; *Kolesov and Geiger*, 2004].

[21] All 10 of these omnipresent bands, as defined by the position of the band emissivity minimum, shift to smaller wave numbers (longer wavelengths) with decreasing Mg content (increasing Fe content) as shown in Figure 1. Numerous previous works show this relationship as well for the Mg-Fe-rich olivines and have correlated the spectral feature positions with the mass and ionic radius of the octahedral cation in the olivine [e.g., *Tarte*, 1963; *Duke and Stephens*, 1964; *Burns and Huggins*, 1972; *Farmer*, 1974; *Jeanloz*, 1980; *Reynard*, 1991; *Hofmeister*, 1987, 1997; *Chopelas*, 1991; *Fabian et al.*, 2001; *Koike et al.*, 2003; *Kolesov and Geiger*, 2004; *Hofmeister and Pitman*, 2007; *Koeppen and Hamilton*, 2008; *Pitman et al.*, 2010; *Hamilton*, 2010]. The variation in position of each of the 10 bands that appear throughout the Mg-Fe solid solution is graphically shown in Figures 6–9. Table 1 also lists the maximum change in wave number position for each of these 10 bands (Δ_{band}). The band(s) that shift the most over the forsterite-fayalite range are bands 6 and 12 that each exhibit a shift (Δ_{band}) of 57 cm^{-1}. Comparison of our spectra with the correlated polarized reflectivity spectra of olivine presented by *Reynard* [1991] indicates that band 6 results from the B_{3u} mode of the ν_4 vibration [also, e.g., *Hofmeister*, 1997; *Fabian et al.*, 2001; *Kolesov and Geiger*, 2004]. Band 12 originates either from the translation of the divalent cation (Mg^{2+} or Fe^{2+}), likely in the B_{2u} polarization [e.g., *Jeanloz*, 1980; *Reynard*, 1991; *Hofmeister*, 1997] or from a ν_2 mode [e.g., *Chopelas*, 1991; *Fabian et al.*, 2001; *Kolesov and Geiger*, 2004]. The minimum difference occurs

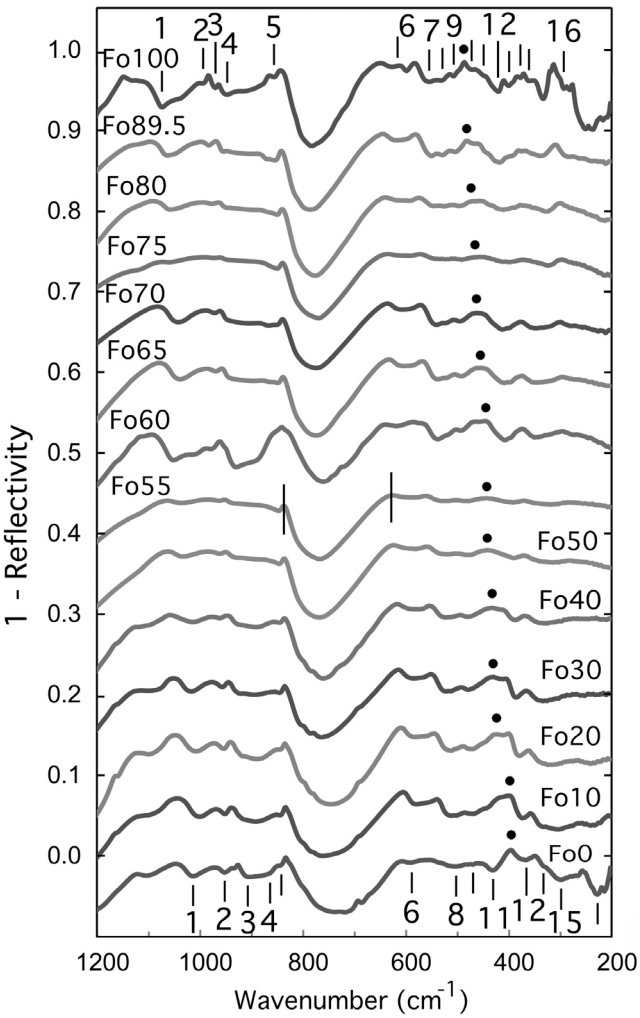

Figure 4. Diffuse reflectivity spectra of powdered synthetic Mg-Fe olivines across the solid solution series. Reflectivity values (R) may be compared with emissivity values (ε) according to Kirchhoff's Law ($\varepsilon = 1 - R$). Vertical lines at Fo_{55} indicate an example of the positions of the band width measurements of the transparency feature. Black dots indicate flection position. Spectra are offset for clarity. Band numbers are noted.

for band 5 (ν_1), showing a Δ_{band} of only 11 cm^{-1}, as predicted by *Chopelas* [1991] using factor group analysis (whose mode must compress the adjacent Mg- or Fe-octahedra [*Hofmeister and Mao*, 2002] that bond the silica tetrahedral together) [e.g., *Servoin and Piriou*, 1973; *Iishi*, 1978; *Piriou and McMillan*, 1983; *Hofmeister*, 1987; *Kolesov and Geiger*, 2004].

[22] The relationship between olivine Mg-Fe solid solution chemistry ($Fo_{\#}$) and fundamental band positions is plotted in Figures 6–9. Linear regression lines (Table 6) were fit to the thermal emissivity bands that are traceable across the solid solution series in order to identify the relationship between olivine composition and wave number position; the resulting R^2 values, as well as their corresponding 2σ values, are shown in Table 1 and Figure 10. The R^2 values for all of the traceable thermal emissivity fundamental bands range between 0.42 and 0.99, and the 2σ values range between 45.45 and 6.73. These values (Table 1) show that for the *best* individual fundamental band (band 12, as judged by highest R^2 and lowest 2σ), the estimation of olivine composition would be accurate to within ±~7 $Fo_{\#}$, but for the *worst* band (band 4) the estimation of olivine composition would be accurate to only ±~45 $Fo_{\#}$. Assessing the 2σ data in Table 1 and Figure 10, for the majority of the fundamental thermal emissivity bands, the composition is show to be estimated to within ±~11–18 $Fo_{\#}$.

4.1.2. Flection Positions in Thermal Emissivity Spectra

[23] Although the emissivity *minima* (and equivalent reflectivity maxima) are reported in the literature and used to determine olivine composition, we find that a certain emissivity *maximum* exists between bands 9 and 10 (or clearly seen, and perhaps more accurately described, between bands 9 and the more obvious band 12 because bands 10 and 11 are not traceable across the entire Mg-Fe solid solution for any technique) in Figure 11 that exhibits an even larger spectral shift as a result of compositional differences (larger than any single emissivity band minimum within this Mg-Fe olivine solid solution series). We call this feature the flection position. This flection position occurs between the higher-frequency internal vibrational modes of the olivine (modes of the SiO_4 tetrahedra) and the lower-frequency external modes (rotational and translational modes of the SiO_4 tetrahedra and translation of the octahedrally coordinated divalent cations from which they are decoupled). This local olivine spectral maximum occurs at 486 cm^{-1} in forsterite and 398 cm^{-1} in fayalite and differs by 88 cm^{-1} between the two end-members (Table 7 and Figure 12). This amount of thermal emissivity flection position shifting is 54% greater than the largest fundamental band shift (of 57 cm^{-1} for both bands 6 and 12). The large shift of this emissivity maximum can be used for the determination of olivine chemistry in the Mg-Fe solid solution series, as can the fundamental emissivity band minima themselves. The relationship between olivine Mg-Fe solid solution chemistry ($Fo_{\#}$) and the flection position is plotted in Figure 12. A linear regression line was fit to the thermal emissivity flection positions (Table 8), and the resulting R^2 value is 0.97 and the 2σ value is 9.93 (Tables 6 and 7), closer to the ideal values of $R^2 = 1$, $2\sigma = 0$ than presented above for any of the fundamental bands, except band 12. The 2σ and R^2 values associated with the flection position mean that 95% of compositional determinations from a measure of flection position will be accurate to within ±~10 $Fo_{\#}$, which is as good as the determinations from some of the best fundamental bands.

4.2. Pressed Pellets: Specular Reflectance and Diffuse Reflectance

4.2.1. Fundamental Band Positions in Specular Reflectivity and Diffuse Reflectivity Spectra

[24] Specular reflectivity and diffuse reflectivity spectra may be compared with thermal emissivity spectra as allowed by Kirchhoff's law ($\varepsilon = 1 - R$), where ε is emissivity and R is reflectivity. Kirchhoff's law is rigorously true only for specular (nonscattering) reflectance data obtained at the higher incidence/emittance angles (highest when normal to the surface) when (lower-angle) Fresnel effects are minimized [e.g., *Salisbury et al.*, 1991a; *Wenrich and Christensen*, 1996; *Hamilton and Minitti*, 2003], or when using an integrating sphere for obtaining directional-hemispherical or

Table 4. Diffuse Reflectance Band Positions for the Forsterite-Fayalite Series (Powders)[a]

	Band Number and Position in This Study (cm^{-1})															
Sample	1 [1]	2 (1) [2]	3 (2)	4 (3) [3]	5 (4) [4]	6 (5) [5]	7 [5a]	8 (6) [6]	9 (7) [7]	10 [8]	11	12 [9]	13 [10]	14 [11]	15 [12]	16 [13]
Fo_{100}	1074	994	970	948	856	617	554	532	507	471	449 sh	419	400	377	360	293
$Fo_{89.5}$	1062	982	953		854	613	549	528	504	468	447 sh	417	389 sh	374	339	285 sh
Fo_{80}	1057	977	952		850	607	544	525	497	464 w	439 sh	411	387 w	371 w	327	
Fo_{75}	1061 w	972	949 w		850	604		520 w	491 w			401			323	
Fo_{70}	1042	971			850 w	603	540	522	495			412		347 w	317 w	280
Fo_{65}	1038	969	937 w		848	600	540	521	493			408	398	347 w	315 w	
Fo_{60}	1051	979		930		612	537	517 w	494			407	394 w	349		273 w
Fo_{55}	1035	962	935 w		847	593	529 w	515 w	478			392		349 w		
Fo_{50}	1032	961	929		846	591	520		479			390			314	
Fo_{40}	1014	961	923	892	845	584	522		479			386			331	
Fo_{30}	1017	957	923	294	845	583	522	513 w	478			385			334	253 w
Fo_{20}	1007	953	918 sh	888	845	577		512	474		sh	379			324	241
Fo_{10}	1000	951	916 sh	892	845	573		512	468		440 sh	374		331	303	240
Fo_0	1013	951	905	865 sh	843 sh	581		502	470 w		431	366		330 sh	297	227
Δ_{band}	74	43	65	83	13	44		30	39		18	53		47	63	66
R^2	0.87	0.87	0.96	0.78	0.86	0.87		0.90	0.90			0.93			0.47	0.98
2σ	18.85	21.58	14.80	33.87	22.71	20.87		19.42	18.57			14.86			45.26	9.97

[a]Band assignments in parentheses are from *Duke and Stephens* [1964]; those in brackets are from *Hamilton* [2010] following *Burns and Huggins* [1972]; abbreviations are sh, shoulder; w, weak; Δ_{band}, maximum difference in band position (in wave number).

hemispherical-directional reflectance of surfaces, thus integrating all of the Fresnel reflection coefficients; diffuse reflectance data have a diffuse component that breaks down the geometric requirements for Kirchhoff's Law to be exactly applied [e.g., *Nicodemus*, 1965; *Hapke*, 1993]. Specular reflectance data must be obtained at high incidence/emittance angles, so that energy from grazing angles is not included at the detector nor distorts the spectrum near the Christiansen frequency, such as can be seen in diffuse reflectance measurements of the our olivine suite spectra (see below) [e.g., *Wenrich and Christensen*, 1996; *Hamilton*, 2010]. Comparison of the thermal emissivity band positions (Table 1) with the specular reflectivity and diffuse reflectivity band positions (that were inverted for comparison with the emissivity data, Tables 2 and 3) shows that the features occur in similar positions (plotted in Figures 6–9), and comparison of Figures 1, 2, 3, and 11 shows that the spectra are quite similar in appearance, too.

[25] Although the pellet spectra from the thermal emission, and specular and diffuse reflection techniques are very similar, the diffuse reflectivity pellet spectra are the most different from the others. For example, Figure 3 exhibits some short-wave variation in the diffuse reflectivity spectra mostly in (but not limited to) the ~1100 to 900 cm^{-1} (~9–11 μm) range, especially in the Fo_{70} spectrum. It is unlikely that this spectral effect in the diffuse reflectance measurements is due to particle size, because all of the samples were ground very finely during synthesis to facilitate complete reaction to form olivine prior to pressing into pellets. Also, all of the pellets were pressed similarly to minimize surface roughness differences. Thus, the high-frequency diffuse reflectivity difference results from some incidence/emittance angles being shallow enough to display Fresnel effects that cause distortion of the spectrum near the Christiansen frequency [e.g., *Salisbury et al.*, 1991a; *Wenrich and Christensen*, 1996; *Hamilton and Minitti*, 2003; *Hamilton*. 2010]. Hence, band 1 diffuse reflectivity data from this study should not be used for compositional determination.

[26] As was seen for thermal emissivity data, bands 6 and 12 in specular and diffuse reflectivity spectra show more

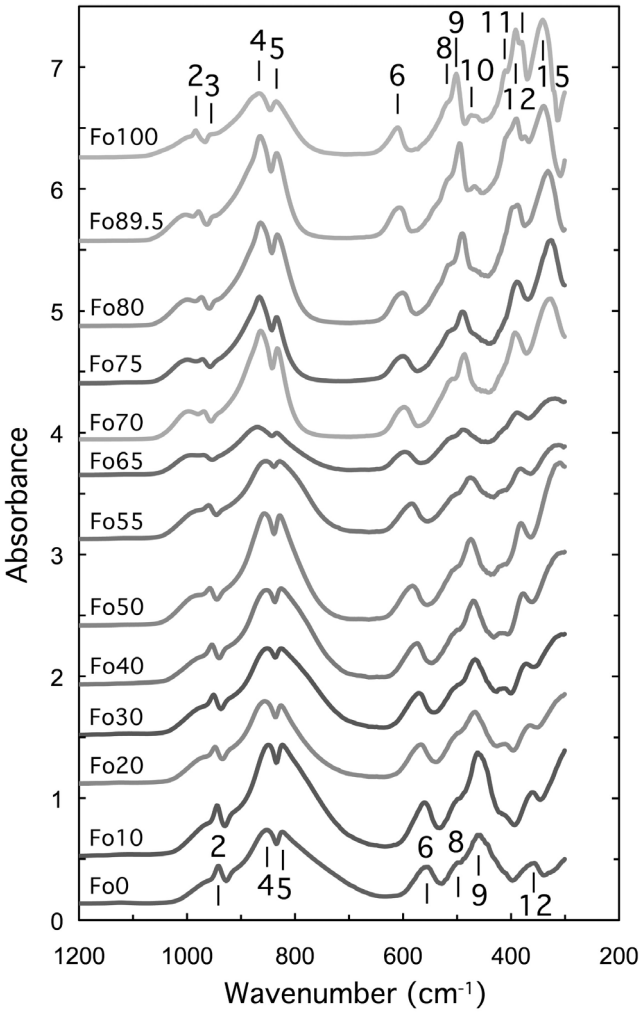

Figure 5. Attenuated total reflectance spectra of powdered synthetic Mg-Fe olivines across the solid solution series. Spectra are offset for clarity. Band numbers are noted.

Table 5. Attenuated Total Reflectance Band Positions for the Forsterite-Fayalite Series (Powders)[a]

	Band Number and Position in This Study (cm^{-1})															
Sample	1 [1]	2 (1) [2]	3 (2)	4 (3) [3]	5 (4) [4]	6 (5) [5]	7 [5a]	8 (6) [6]	9 (7) [7]	10 [8]	11	12 [9]	13 [10]	14 [11]	15 [12]	16 [13]
Fo_{100}	sh	984	958 sh	867	835	610		520 sh	501	474	410	391		381	342	280
$Fo_{89.5}$	1003	979	953 sh	865	834	606		518 sh	495	468	sh	390		374	340	271
Fo_{80}	1000	973	948 sh	864	833	601		516 sh	490		397	388			332	243
Fo_{75}	1000	971		866	834	600		515 sh	490			389			326	237
Fo_{70}	997	969	sh	864	833	598		514 sh	486			392			327	231
Fo_{65}	990	967		870	834	596		514 w	488			389			318	
Fo_{55}	983 w	960		854	828	584		509 w	476			382			312	
Fo_{50}	981 w	958	sh	856	828	583		509 w	475			382			309	221
Fo_{40}	w	954	sh	853	826	574		499 w	470	420		378			w	
Fo_{30}	w	950	sh	851	825	571		w	466	413		372			w	w
Fo_{20}	w	948	sh	856	825	567		w	466	410		365			w	
Fo_{10}	w	945	sh	849	823	561		499 w	462			360				
Fo_{0}	w	942	sh	852	823	554		499 w	460			357				
Δ_{band}		42		18	12	56		21	41			34				
R^2	0.93	0.98		0.62	0.91	0.99		0.90	0.96			0.91			0.92	0.92
2σ	6.61	8.12		34.90	17.78	6.86		18.01	11.63			18.04			8.63	7.89

[a]Band assignments in parentheses are from *Duke and Stephens* [1964]; those in brackets are from *Hamilton* [2010] following *Burns and Huggins* [1972]; abbreviations are sh, shoulder; w, weak; Δ_{band}, maximum difference in band position (in wave number).

variation in position from forsterite to fayalite than any of the other fundamental bands (Δ_{band} = 59 and 57 cm^{-1}, respectively, for specular reflectivity data; Δ_{band} = 64 and 59 cm^{-1}, respectively, for diffuse reflectivity data). Also, similarly to the thermal emissivity data, band 5 shows the least variation in position for both specular reflectivity and diffuse reflectivity data (12 cm^{-1} for each). However, the R^2 and 2σ specular reflectivity values for band 6 are poor and only moderate for the diffuse reflectivity data, raising doubt as to the efficacy of using band 6 for compositional determination.

[27] Figures 6–9 show the relationship between olivine Mg-Fe solid solution chemistry ($Fo_{\#}$) and fundamental band positions (for specular reflectivity, diffuse reflectivity, and thermal emissivity data). Linear regression lines were fit to the specular reflectivity and diffuse reflectivity bands, and the resulting R^2 values, as well as their corresponding 2σ values, are shown in Tables 2 and 3 and Figure 10. The R^2 values for all of the traceable specular reflectivity fundamental bands range between 0.18 and 0.97 and the 2σ values range between 54.08 and 10.25. The R^2 values for all of the traceable diffuse reflectivity fundamental bands range between 0.37 and 0.99, and the 2σ values range between 47.58 and 7.18. The R^2 values (Tables 2 and 3, Figure 10) show that for the *best* individual fundamental band (specular reflectivity = band 9; diffuse reflectivity = band 9, as judged by highest R^2 and lowest 2σ), the estimation of olivine composition would be accurate to within ±~7–10 $Fo_{\#}$, but for the *worst* band (specular reflectivity = band 4; diffuse reflectivity = band 4) the estimation of olivine composition would be accurate to only ±~47–54 $Fo_{\#}$. Assessing the 2σ data in Tables 2 and 3, it is shown that for the majority of the fundamental specular reflectivity and diffuse reflectivity bands, the composition would be estimated to within ±~9–17 $Fo_{\#}$.

4.2.2. Flection Positions in Specular Reflectivity and Diffuse Reflectivity Spectra

[28] The relationship between olivine Mg-Fe solid solution chemistry ($Fo_{\#}$) and the specular reflectivity and diffuse reflectivity flection positions is shown in Figures 11 and 12. As noted for the thermal emissivity data, the flection position in the specular reflectivity and diffuse reflectivity spectra also shifts more ($\Delta_{flection}$ = 89 cm^{-1} for both specular reflectivity and diffuse reflectivity spectra) than the largest fundamental band does. For the specular reflectivity data, the local olivine flection maximum occurs at 487 cm^{-1}

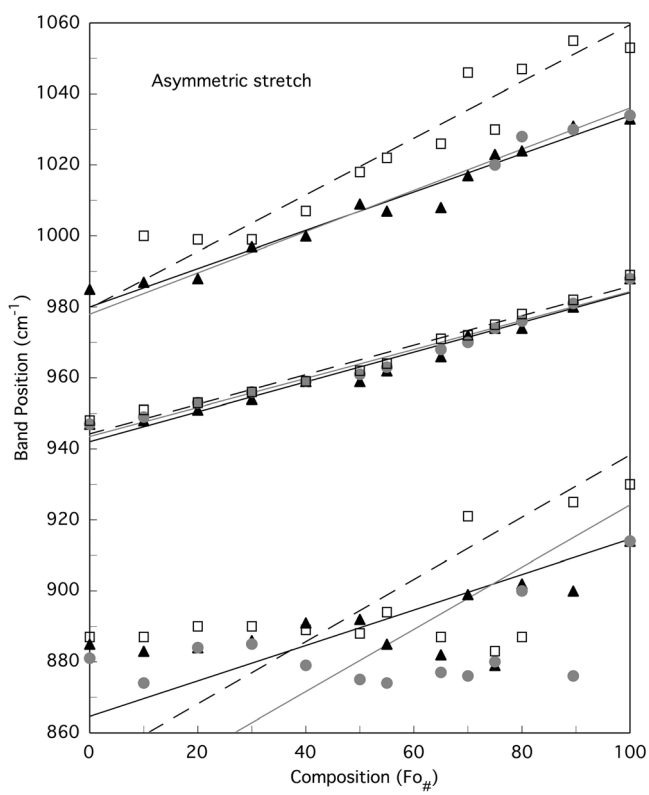

Figure 6. Asymmetric stretching band positions (ν_3) as they vary with composition for each technique (thermal infrared emission (black triangles with black lines), specular reflectance (gray circles with gray lines), and diffuse reflectance (open squares with dashed lines)). Top to bottom are bands 1, 2, and 4.

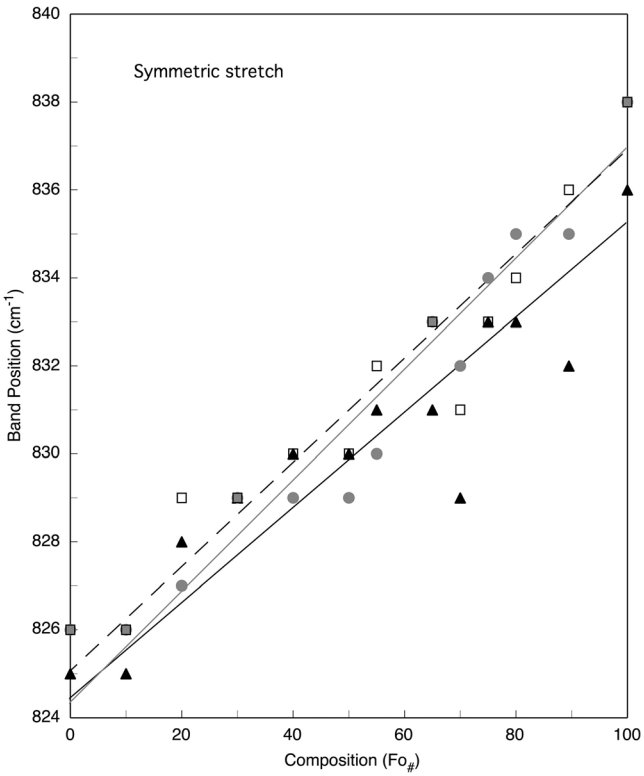

Figure 7. Symmetric stretching band position (ν_1) as it (band 5) varies by composition for each technique (thermal infrared emission (black triangles with black line), specular reflectance (gray circles with gray line), and diffuse reflectance (open squares with dashed line)).

in forsterite and 398 cm^{-1} in fayalite (Table 7 and Figure 12). This amount of specular reflectivity flection position shifting is 51% greater than the largest fundamental band shift (of 59 cm^{-1} for band 6). For the diffuse reflectivity data, the local olivine flection maximum occurs at 488 cm^{-1} in forsterite and 399 cm^{-1} in fayalite and also differs by 89 cm^{-1} between the two end-members (Table 7 and Figure 12). This amount of diffuse reflectivity flection position shifting is 39% greater than the largest fundamental band shift (of 64 cm^{-1} for band 6). Linear regression lines were fit to the specular reflectivity and diffuse reflectivity flection positions (Table 8) and the resulting specular reflectivity R^2 value is 0.94 and the 2σ value is 14.89; the diffuse reflectivity R^2 value is 0.97 and the 2σ value is 10.15 (Tables 6 and 7). The 2σ and R^2 values associated with the flection position means that for the specular reflectivity data, ~95% of compositional determinations from a measure of flection position will be accurate to within ±~15 $Fo_{\#}$; for the diffuse reflectivity data, ~95% of compositional determinations from a measure of flection position will be accurate to within ±~10 $Fo_{\#}$. These values are on par with the compositional determinations using the fundamental band positions.

4.3. Powders: Diffuse Reflectance

4.3.1. Fundamental Band Positions in Diffuse Reflectivity Powder Spectra

[29] Diffuse reflectivity spectra of the powdered olivine sample suite are shown in Figure 4. These sample spectra show typical spectral behaviors related to particle size, including substantially decreased spectral contrast in the fundamental (Reststrahlen) bands (which still occur in the same general spectral position as those associated with the pressed pellets, Figure 3) and the appearance of increased spectral contrast in the transparency regions due to multiple and volume scattering that occurs between the fundamental band regions (related to the material's complex index of refraction). For example, the increased reflectivity (which would correspond to decreased emissivity) at wave numbers larger than ~1150 cm^{-1} and the most prominent feature in the spectra (at ~800 cm^{-1}) result from multiple and volume scattering related to the fine particle size of the powdered (and unpressed) samples [e.g., *Lyon*, 1964; *Aronson et al.*, 1966; *Hunt and Vincent*, 1968; *Vincent and Hunt*, 1968; *Conel*, 1969; *Hunt and Logan*, 1972; *Aronson and Emslie*, 1973; *Salisbury and Eastes*, 1985; *Moersch*, 1992; *Salisbury and Wald*, 1992; *Gaffey et al.*, 1993b; *Wald*, 1999; *Moersch and Christensen*, 1995; *Wald and Salisbury*, 1995; *Mustard and Hays*, 1997; *Lane and Christensen*, 1998; *Lane*, 1999; *Cooper et al.*, 2002].

[30] Spectral features arise largely from the interaction of light and the surfaces of particles. In fine-particulate samples, the small particle diameters and increased interfaces per unit volume allow more energy to pass through each grain and increase the number of grain surface reflections that can occur (both internal and external). This behavior is

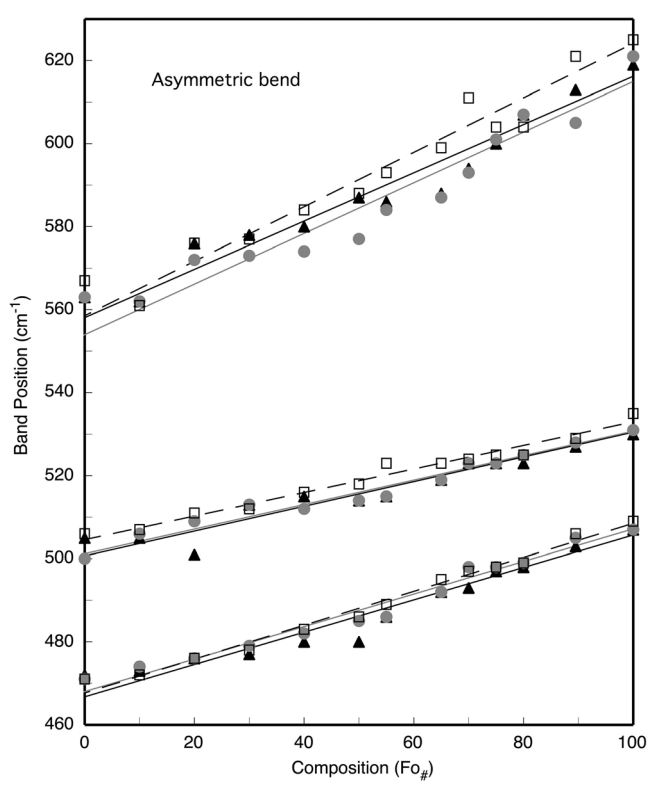

Figure 8. Asymmetric bending band positions (ν_4) as they vary by composition for each technique (thermal infrared emission (black triangles with black lines), specular reflectance (gray circles with gray lines), and diffuse reflectance (open squares with dashed lines)). Top to bottom are bands 6, 8, and 9.

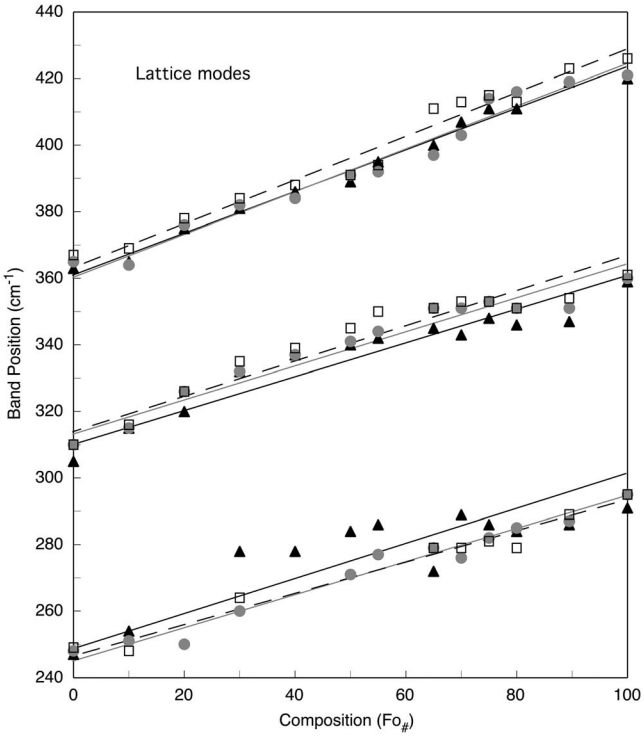

Figure 9. Lattice mode band positions as they vary by composition for each technique (thermal infrared emission (black triangles with black lines), specular reflectance (gray circles with gray lines), and diffuse reflectance (open squares with dashed lines)). Top to bottom are bands 12, 15, and 16.

unlike that in the pressed pellet samples, for which pressing creates effectively larger and fewer particles and reduces these scattering effects. Our diffuse reflectivity olivine-powder results are similar to the spectra of hyperfine olivine particles presented by *Mustard and Hays* [1997], who presented a detailed discussion of olivine (and quartz) spectra as they relate to particle size.

[31] For powdered samples, the fundamental reflectance features are muted and, although migration trends in the positions of these bands (Table 4) are similar to the pelletized samples, the bands are weak and are difficult to use for compositional determination. Despite exhibiting weaker fundamental bands, the diffuse reflectivity powdered sample data exhibit an additional band (ν_3) (band 3) that is traceable throughout the Mg-Fe solid solution series, bringing the total number of traceable bands to 11 (Table 4). Linear regression lines were fit to the powdered sample diffuse reflectivity fundamental bands and the resulting R^2 and 2σ values are shown in Table 4. The R^2 values for all of the traceable diffuse reflectivity fundamental bands range between 0.47 and 0.98, and the 2σ values range between 45.26 and 9.97. These values (Table 4) show that for the *best* individual fundamental band (band 3; band 16 was better but was considered to have too many undefined values), the estimation of olivine composition would be accurate to within ±~15 $Fo_{\#}$, but for the *worst* band (band 15) the estimation of olivine composition would be accurate to only ±~45 $Fo_{\#}$. Assessing the 2σ data in Table 4, it is shown that for the majority of the fundamental diffuse reflectivity powder bands, the composition would be estimated to within ±~15–23 $Fo_{\#}$.

4.3.2. Transparency Band Positions in Diffuse Reflectivity Powder Spectra

[32] Because of the weakness of the fundamental bands, a better measure of olivine composition in the fine-particulate diffuse reflectivity spectra (Figure 4) may be the obvious transparency feature at ~800 cm^{-1}. The utility of transparency features and "weak bands" in fine-grained mineral spectra for compositional analysis has been described before in the literature [e.g., *Salisbury et al.*, 1987; *Nash and Salisbury*, 1991; *Wagner*, 2000; *Cooper et al.*, 2002], but mostly in terms of using the Christiansen frequency whose

Table 6. Linear Regression Equations Used to Fit Band Positions for the Spectral Data in Tables 1–5[a]

Technique	Band	Regression Equation
TE (pellet)	1	$f(y) = 1.85y - 1817.03$
	2	$f(y) = 2.38y - 2243.79$
	4	$f(y) = 2.00y - 1730.14$
	5	$f(y) = 9.24y - 7615.78$
	6	$f(y) = 1.72y - 959.87$
	8	$f(y) = 3.35y - 1679.09$
	9	$f(y) = 2.56y - 1196.86$
	12	$f(y) = 1.60y - 576.69$
	15	$f(y) = 1.97y - 610.83$
	16	$f(y) = 1.90y - 471.39$
SR (pellet)	1	$f(y) = 1.72y - 1683.22$
	2	$f(y) = 2.45y - 2312.16$
	4	$f(y) = 1.14y - 954.35$
	5	$f(y) = 7.92y - 6528.48$
	6	$f(y) = 1.64y - 907.98$
	8	$f(y) = 3.39y - 1696.92$
	9	$f(y) = 2.55y - 1193.46$
	12	$f(y) = 1.56y - 560.84$
	15	$f(y) = 1.96y - 612.43$
	16	$f(y) = 2.01y - 492.46$
DR (pellet)	1	$f(y) = 1.25y - 1227.26$
	2	$f(y) = 2.40y - 2270.18$
	4	$f(y) = 1.14y - 969.98$
	5	$f(y) = 8.44y - 6960.23$
	6	$f(y) = 1.52y - 851.53$
	8	$f(y) = 3.52y - 1774.86$
	9	$f(y) = 2.45y - 1143.95$
	12	$f(y) = 1.52y - 553.35$
	15	$f(y) = 1.89y - 593.14$
	16	$f(y) = 2.13y - 524.06$
DR (powder)	1	$f(y) = 1.22y - 1212.69$
	2	$f(y) = 2.43y - 2295.97$
	3	$f(y) = 1.83y - 1658.82$
	4	$f(y) = 0.70y - 597.44$
	5	$f(y) = 7.48y - 6293.05$
	6	$f(y) = 1.94y - 1103.65$
	8	$f(y) = 3.75y - 1889.20$
	9	$f(y) = 2.26y - 1045.34$
	12	$f(y) = 1.72y - 628.79$
	15	$f(y) = 1.34y - 379.88$
	16	$f(y) = 1.53y - 351.86$
ATR (powder)	1	$f(y) = 1.52y - 1439.67$
	2	$f(y) = 2.37y - 2224.09$
	4	$f(y) = 2.95y - 2487.42$
	5	$f(y) = 6.34y - 5204.78$
	6	$f(y) = 1.69y - 936.86$
	8	$f(y) = 3.76y - 1862.89$
	9	$f(y) = 2.24y - 1019.30$
	12	$f(y) = 2.41y - 863.12$
	15	$f(y) = 1.37y - 375.76$
	16	$f(y) = 0.64y - 81.17$

[a]Parameters are $f(y)$, composition ($Fo_{\#}$); y, wave number position.

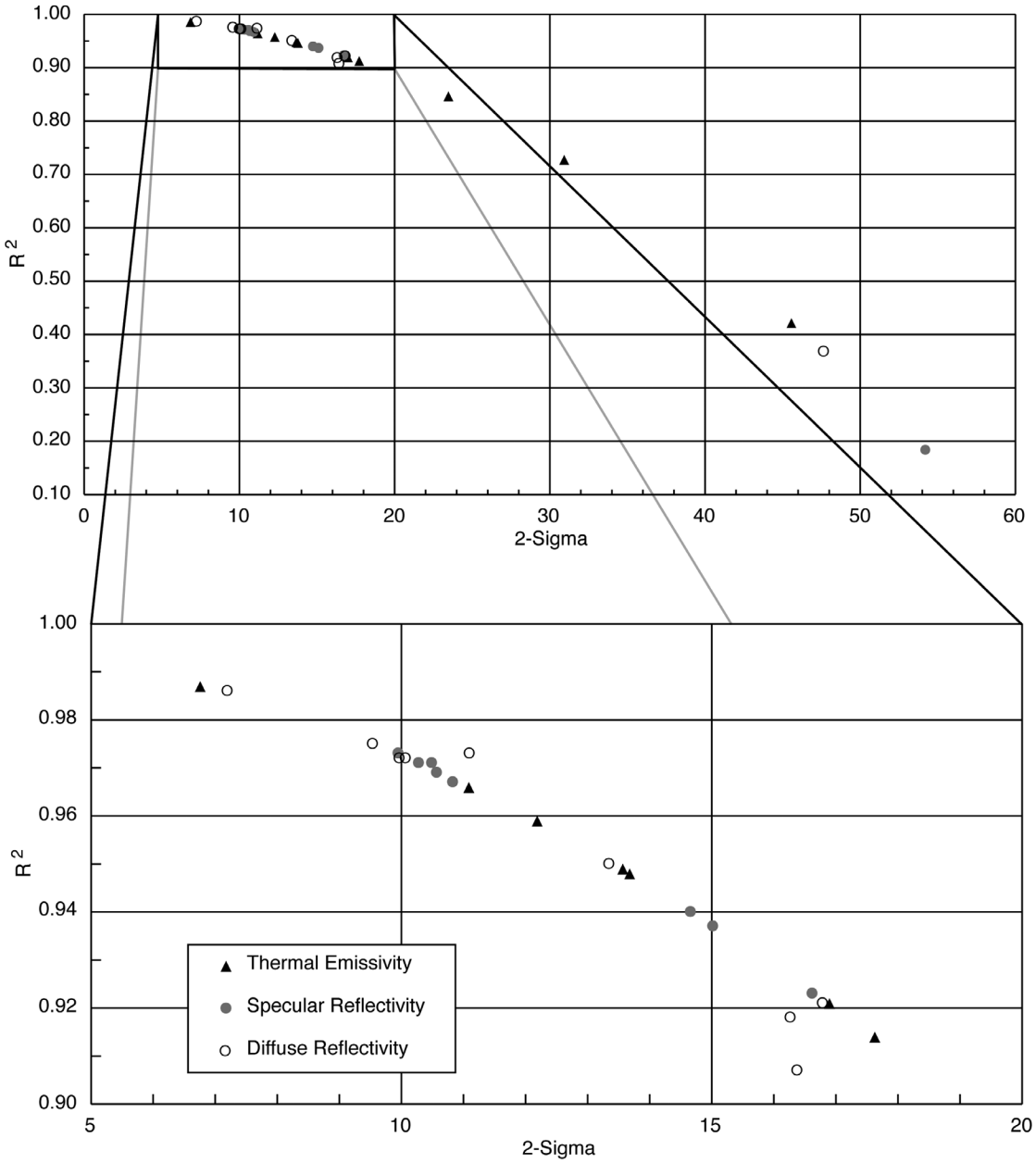

Figure 10. Relationship between R^2 and 2σ for the (upper) fundamental band shifts for each pellet technique (thermal infrared emission (black triangles), specular reflectance (gray circles), and diffuse reflectance (open squares)); with an (lower) expanded view of a subset of the graph showing the majority of the points.

position becomes very clear when spectra of multiple particle sizes (but similar chemistry) are plotted. Here we note that the predominant olivine transparency feature in our spectral data shifts in wavelength position with olivine composition as do the weakened Reststrahlen bands, and we also find that the transparency feature is narrower in the Fo_{100} spectrum and broader in the Fo_0 spectrum (Figures 4 and 13). The width of this feature was measured using the low-reflectivity locations on each side of the volume scattering feature and was found to be 195 cm^{-1} wide for forsterite (between 843 and 648 cm^{-1}) and 227 cm^{-1} wide for fayalite (between 833 and 606 cm^{-1})–a difference of 32 cm^{-1}. This "band width" (W, in cm^{-1}) variation is mapped well by a linear fit according to the equation $Fo_{\#} = -2.54\ W + 590.32$ (Figure 13). For this equation, $R^2 = 0.95$ and 2σ is 12.8. This 2σ value means that 95% of compositional determinations from a measure of band width will be accurate to within ±~13 $Fo_{\#}$ (for particles similar to those used in this study (<45 μm in diameter)). Transparency band width behavior was not studied further because there were no other synthetic olivine samples of different particle sizes for analysis.

4.3.3. Flection Positions in Diffuse Reflectivity Powder Spectra

[33] As seen in the thermal emissivity, specular reflectivity, and diffuse reflectivity pellet spectra (Figures 1–3

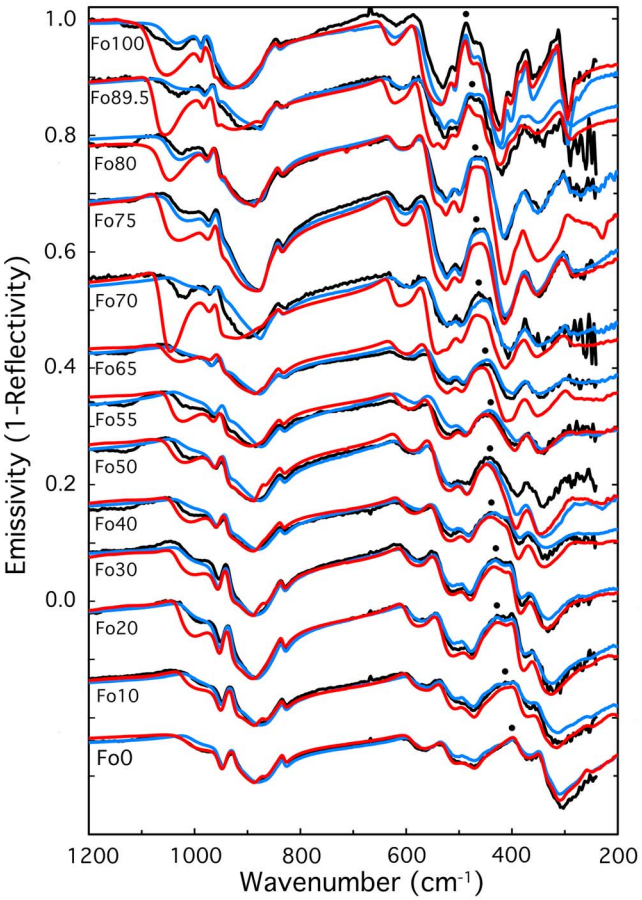

Figure 11. Thermal emissivity (black), specular reflectance (blue), and diffuse reflectance (red) spectra of pressed pellets made from synthetic Mg-Fe olivines across the solid solution series. The flection positions of the thermal emissivity spectra are identified by the black dots and show how this emissivity maximum (reflectivity minimum) shifts across the Mg-Fe olivine suite in a similar manner to the fundamental (Reststrahlen) bands. The specular reflectivity and diffuse reflectivity pellet spectra have been scaled to the thermal emissivity spectra. Spectra are offset for clarity. The flection points for the specular and diffuse reflectance data were similarly determined and varied slightly from the thermal emissivity data (see Figure 12); however, their positions are not shown by dots in this figure for clarity.

and 11), the diffuse reflectivity powdered data also show a flection position that migrates more than any single band over the Mg-Fe solid solution (Table 7 and Figure 4). For these powdered samples, the position of the low-reflectivity flection shifts from 486 cm^{-1} (forsterite) to 395 cm^{-1} (fayalite), a change in position of 91 cm^{-1}. Compared in a similar way as the other data sets, this amount of flection point shifting is a mere 10% greater than the largest fundamental band shift (of 83 cm^{-1} for band 4). However, band 4 has a very low R^2 value (of 0.78) and a very large 2σ value (of 33.87) compared with the rest of the bands; because of this character and the fact that the band 4 linear regression is based on many undefined band position values for band 4 (Table 4), we consider band 4 an outlier data point, and thus

Table 7. Flection Band Positions for the Forsterite-Fayalite Series for Several Techniques[a]

Sample	TE (Pellet)	SR (Pellet)	DR (Pellet)	DR (Powder)	ATR (Powder)
Fo_{100}	486	487	488	486	486
$Fo_{89.5}$	476	479	482	481	480
Fo_{80}	469	467	467	471	476
Fo_{75}	468	456	460	467	440
Fo_{70}	463	456	465	462	442
Fo_{65}	451	447	456	454	443
Fo_{60}				445	
Fo_{55}	442	443	450	443	433
Fo_{50}	443	441	448	441	438
Fo_{40}	441	432	444	432	432
Fo_{30}	430	432	435	430	426
Fo_{20}	428	428	428	422	426
Fo_{10}	413	423	414	398	394
Fo_0	398	398	399	395	398
Δ_{band}	88	89	89	91	92
R^2	0.97	0.94	0.97	0.98	0.87
2σ	9.93	14.89	10.15	8.64	21.85

[a]Δ_{band}, maximum difference in flection position (in wave number).

compare the results of the flection position shift with the band with the second-highest Δ_{band} value (which is band 1). Band 1 varies in position from Fo_{100} to Fo_0 by 74 cm^{-1}, so the flection point shift ($\Delta_{flection}$ = 91 cm^{-1}) can be calculated

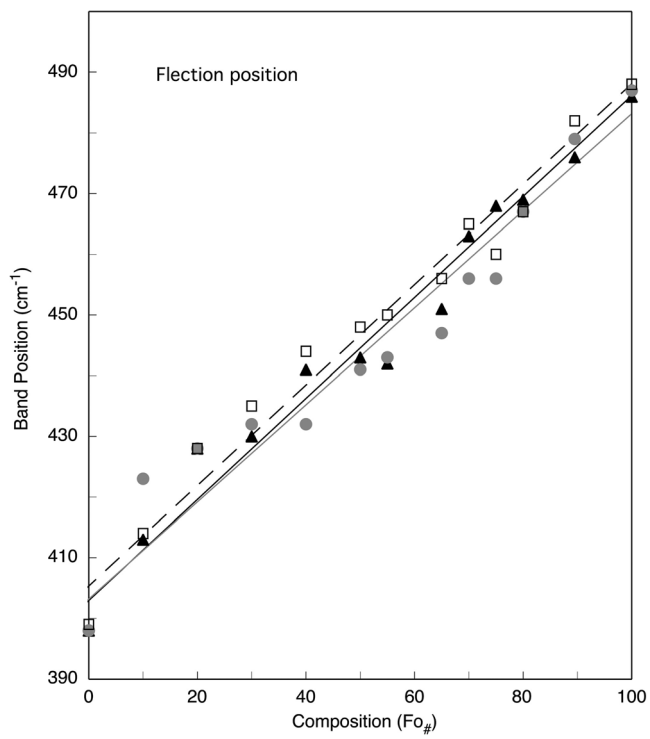

Figure 12. Flection position (i.e., the emissivity maximum (reflectivity minimum)) as it varies by olivine composition for each technique (thermal infrared emission (black triangles with black line), specular reflectance (gray circles with gray line), and diffuse reflectance (open squares with dashed line)). This flection position varies over the range of Mg-Fe solid solution more than any olivine fundamental band minimum (for all of the techniques) and may be exploited for determining Mg-Fe solid solution composition.

Table 8. Linear Regression Equations Used to Fit Flection Positions for the Spectral Data in Table 7[a]

Technique	Regression Equation
TE (pellet)	$f(y) = 1.20y - 484.19$
SR (pellet)	$f(y) = 1.25y - 504.07$
DR (pellet)	$f(y) = 1.21y - 489.67$

[a]Parameters are $f(y)$, composition ($Fo_{\#}$); y, wave number position.

to be 23% greater than the "largest" fundamental band shift. The linear regression fit to the powdered diffuse reflectivity flection position data has an R^2 value of 0.98 and a 2σ value of 8.64 (Tables 6 and 7). The 2σ and R^2 values associated with the diffuse reflectivity flection position means that 95% of compositional determinations from a measure of flection position will be accurate to within ±~9 $Fo_{\#}$.

4.4. Powders: Attenuated Total Reflectance

4.4.1. Fundamental Band Positions in Attenuated Total Reflectivity Powder Spectra

[34] The attenuated total reflectivity spectral data were acquired of loose powders (Figure 5). Band positions in the attenuated total reflectivity spectra (Table 5) typically occur at slightly lower frequencies (smaller wave numbers) than other spectral techniques, because ATR absorbance (using an evanescent wave) measures only the imaginary part of the complex refractive index (unlike emission or reflectance techniques that measure both the real and imaginary indices [n and k] of minerals) [e.g., *Harrick*, 1967; *Young and Rothrock*, 1963; *Chemtob et al.*, 2010].

[35] Seven bands (bands 2, 4, 5, 6, 8, 9, and 12) are traceable across the entire Mg-Fe olivine suite (Table 5). Three additional bands (bands 1, 15, and 16) are traceable only from Fo_{100} to Fo_{50} and their results are also reported. The smallest change in wave number position across the entire Mg-Fe series is associated with band 5 ($\Delta_{band} = 12$ cm^{-1}), and the largest change in position is band 6 ($\Delta_{band} = 56$ cm^{-1}); these band behaviors also are common in the other techniques (Tables 1–4) as discussed previously.

[36] Linear regression lines were fit to the powdered sample ATR bands (Figure 5) and the resulting R^2 and 2σ values are shown in Table 5. The R^2 values for all of the traceable ATR fundamental bands range between 0.62 and 0.99, and the 2σ values range between 34.90 and 6.61. The values on Table 5 show that for the *best* individual fundamental band (band 6), the estimation of olivine composition would be accurate to within ±~7 $Fo_{\#}$, but for the *worst* band (band 4) the estimation of olivine composition would be accurate to only ±~35 $Fo_{\#}$. Assessing the 2σ data in Table 5, it is shown that for the majority of the fundamental ATR bands, the composition would be estimated to within ±~7–18 $Fo_{\#}$.

4.4.2. Flection Positions in Attenuated Total Reflectivity Powder Spectra

[37] Another trend seen in the attenuated total reflectivity data that resembles the spectral behavior of the other techniques is that the flection position (Table 7) between bands 9 and 12 varies over a broader wave number range than that of any individual band. For the attenuated total reflectivity data, this change is 92 cm^{-1} (Table 7), with slightly more scatter than the other techniques. This amount of attenuated total reflectivity flection position shifting is 64% greater than the largest fundamental band shift (of 56 cm^{-1} for band 6). Linear regression lines were fit to the ATR flection positions, and the resulting R^2 value is 0.87 and the 2σ value is 21.85 (Tables 6 and 7). The 2σ and R^2 values associated with the flection position mean that 95% of compositional determinations from a measure of flection position will be accurate to within ±~22 $Fo_{\#}$.

5. Discussion

[38] The synthetic olivine spectra from five data sets acquired using four different midinfrared techniques (thermal emission, specular reflectance, diffuse reflectance (pellets and powders), and attenuated total reflectance powders) have been presented in order to determine how the fundamental bands shift with changes in Mg-Fe olivine composition. A sample suite that was well populated by 13 chemical subdivisions in the Mg-Fe solid solution series (14 for the powdered diffuse reflectivity data) enabled 10 spectral bands to be well traced from forsterite to fayalite for all spectral techniques (for the diffuse reflectivity powdered spectra we identified 11 fully traceable bands, and for the attenuated total reflectance powdered spectra, only 7 bands were fully traceable over the Fo_{100} to Fo_0 range, but 3 additional bands were traceable from Fo_{100} to Fo_{50}).

[39] Although the main purpose of this paper is to chronicle the midinfrared band behaviors of a suite of synthetic Mg-Fe olivines of many pure chemical subdivisions using many spectral techniques, a subordinate objective for this work is to determine the utility of applying these diverse laboratory spectra to predict olivine composition. There are three

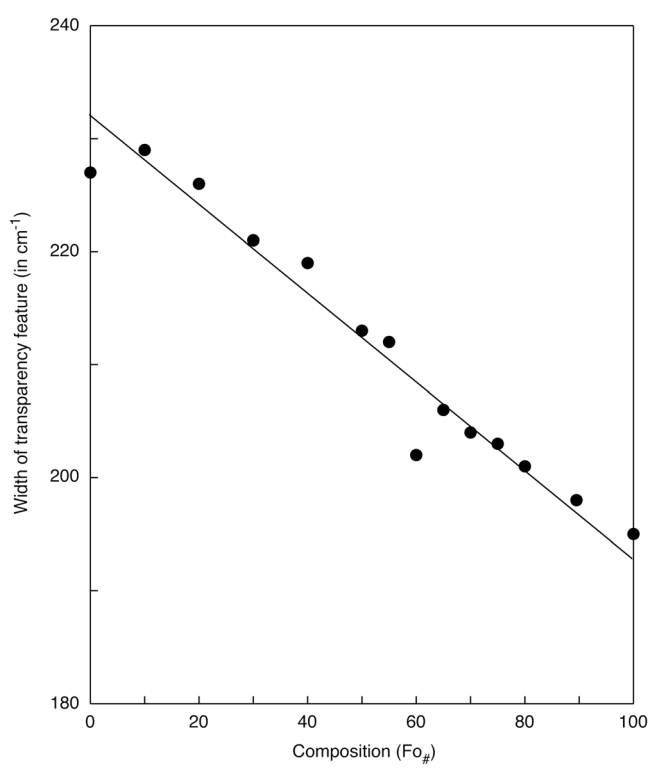

Figure 13. Width of the transparency band as it varies with composition across the Mg-Fe solid solution olivine series. $R^2 = 0.95$; $2\sigma = 12.84$.

strategies applied in the literature for correlating spectral character to olivine composition. One strategy is to study the position of the fundamental spectral bands [e.g., *Tarte*, 1963; *Duke and Stephens*, 1964; *Burns and Huggins*, 1972; *Jäger et al.*, 1998; *Koike et al.*, 2003; *Tarantino et al.*, 2003; *Hamilton*, 2010], one is to study the position of the Christiansen frequency (CF) [*Hofmeister and Pitman*, 2007; *Hamilton*, 2010], and one strategy uses fundamental bandwidths to determine composition [*Hofmeister and Pitman*, 2007]. Typically combinations of these strategies are considered together [e.g., *Hofmeister and Pitman*, 2007; *Hamilton*, 2010]. In this work, we have not examined the CF relationship in our synthetic olivine spectra; however, we have studied in great detail the spectral behavior of the fundamental bands and in one case (diffuse reflectivity spectra of powdered olivine) we analyzed the width of the transparency band as it varied with composition. Furthermore, we have studied what we are calling the flection position that migrates with chemical composition (i.e., a specific emissivity maximum/reflectance minimum position as it varies with $Fo_{\#}$) and suggest that this flection position may be another viable means of identifying olivine composition in an unknown spectrum, especially in a fine-grained sample whose fundamental band features would be subdued.

5.1. Linear Regression Analyses of Fundamental Band Positions

[40] We applied linear regressions to the band position data (Tables 1–5) to determine the goodness of fit (R^2) of our data to the olivine composition ($Fo_{\#}$). *Hofmeister and Pitman* [2007] and *Pitman et al.* [2010] noted that many of the trends for olivine bands (measured in transmission) were better fit by two linear segments with different slopes at ~Fo_{70}. *Hofmeister and Pitman* [2007] suggest that the change in slope results from changes in bond length associated with the larger Fe ion substituting for the smaller Mg cation and distorting the "oxygen sublattice about the impurity site." *Koike et al.* [2003] found a linear relationship for most of the midinfrared, but noted that for the longer-wavelength region of the data into the far-infrared (~145–300 cm^{-1}) linearity occurs near the end-members, but not in the middle compositional range (~$Fo_{40–60}$). We did not identify a need for applying more than one linear equation to our data because of the scatter (nor did *Duke and Stephens* [1964], *Burns* [1970], *Burns and Huggins* [1972], *Huggins* [1973], or *Tarantino et al.* [2003]).

[41] For the pelletized samples (measured in thermal emission, specular reflectance, and diffuse reflectance), by far, our worst fitting data to a linear regression were associated with the shifting of band 4 (Tables 1–3). The R^2 values were the lowest and the 2σ values were the highest of the 10 traceable bands for each spectral measurement technique. This poor fit occurred because band 4 is broad and rounded, not narrow and sharp, making the band minimum (Figures 1–3) move around significantly (and not in a uniform direction) from forsterite to fayalite, due to the stronger influence of various polarizations of the band. *Fabian et al.* [2001] show that in this band 4 region, particle shape can dramatically affect the peak position as well. The 2σ values for band 4 (45.45, 54.08, and 47.58; average = 49.04) suggest that if the band 4 wave number position alone were used for estimating olivine composition, the chemistry could be wrong by almost 50 mol % Fo. For the powdered samples, the 2σ values of band 4 were the highest (attenuated total reflectivity) or the second highest (diffuse reflectivity) of all of the bands: evidence to poor fit of the data to a line (and verified by fairly low R^2 values (Tables 4 and 5)). A summary analysis by *Hamilton* [2010] of five previous olivine transmission studies also showed that, of the traceable forsterite-fayalite bands, this particular band (called "band 3" in that paper) returned the poorest goodness of fit and largest standard error, too (for transmission data (most akin to our attenuated total reflectance data) but not for reflection or emission data).

[42] *Burns and Huggins* [1972] suggested that the best bands for determining olivine composition in natural samples were those equivalent to our bands 5 and 6, because they are "sharp, relatively free from overlap with neighboring bands, and also show an adequate frequency range." Although our band 5 [ν_1] is sharper and clearer in position than other bands, its position does not vary much over the full suite from forsterite to fayalite (Δ_{band} = 11–13 cm^{-1}); the band 5 R^2 and 2σ values for all of our techniques are always in the bottom third of the values (i.e., away from the ideal values of $R^2 = 1$, $2\sigma = 0$) (Tables 1–5), so band 5 generally may not be better than other bands for estimating composition. Band 6 routinely exhibited a large change in band position with change in chemical composition (Δ_{band} = 44–64 cm^{-1}), but the band 6 R^2 and 2σ values ranged from the bottom half of the values (for specular reflectivity, diffuse reflectivity, and diffuse reflectivity of powders), to midrange values (for thermal emissivity), to better values (attenuated total reflectivity) (Tables 1–5). Thus band 6 may be better than band 5 for estimating composition, but generally may not be the best band for that task.

[43] In the olivine spectroscopy review paper, *Hamilton* [2010, p. 11] argued that bands with high R^2 values "should be the best bands for determination of accurate Mg-Fe composition" (as presented for transmission data and shown to be effective for other data sets). Hamilton combined band positions from many different olivine spectroscopy studies into one data set and noted that the summarized band data have "strong linear correlations" (R^2 from 0.760 to 0.963 for eight different bands). Strong linearity (an indication for lack of ordering of the Mg^{2+} and Fe^{2+} into the M1 and M2 sites [*Burns and Huggins*, 1972]) also is seen for the synthetic olivine spectra presented here. Tables 1–5 and 7 list the R^2 values for each band and the flection positions. The R^2 values were determined through linear fits of the data as shown in Figures 6–9 and 11. For the thermal emissivity, specular reflectivity, and diffuse reflectivity pellet data, our bands with the highest R^2 values were band 12 (0.99) (which exhibits a routinely large Δ_{band}), band 9 (0.97), and band 9 (0.99), respectively (Tables 1–3). For the powdered data the bands with the highest R^2 values were band 16 (0.98) and band 6 (0.99) for the diffuse reflectivity and attenuated total reflectivity spectra, respectively (Tables 4–5). In order, the associated 2σ values were 6.73, 9.92, 7.18, 9.97, and 6.86 (i.e., ~7–10). These low-error values imply that for 95% of the efforts to identify olivine composition using these specific bands, the composition would be correctly predicted within ±7–10 mol % Fo. These bands represent our best case scenarios. The 2σ values from Tables 1–3 (as plotted against R^2) are shown in Figure 10 for the thermal emissivity, specular reflectivity, and diffuse reflectivity

pellet data. The positions of the majority of these data points (22 of 29) indicate that, in general, these spectral techniques can be used to predict olivine composition to ±9–18 mol % Fo using fundamental band position (2 points are better than that estimation, 5 points are worse).

[44] These values are similar to those found in the review paper of *Hamilton* [2010]. *Hamilton* [2010] states the prediction value of ±6–10 mol % Fo using the combined transmission bands of *Duke and Stephens* [1964], *Burns and Huggins* [1972], *Salisbury et al.* [1991b], *Koike et al.* [2003], and *Hofmeister and Pitman* [2007] and ±9–15 mol % Fo for the best transmission band-depth ratio data of *Hofmeister and Pitman* [2007]. *Hamilton* [2010] also shows olivine prediction values of ±5.6–7.3 mol % Fo in her Table 4 for the best five bands in reflectance data of *Clark et al.* [2007] and shows ±2.5–5.7 mol % Fo in her Table 7 for the best five bands for smoothed emissivity data).

[45] We suggest that invoking a high R^2 value to identify a good band for ascertaining $Fo_{\#}$ is not necessarily the best approach for determining composition. If the wave number value shifts only slightly over the forsterite-fayalite solid solution (small Δ_{band}), but the data points fall well on a linear regression line, the R^2 value will be high, but there can be a lot of uncertainty in determining the $Fo_{\#}$ with confidence if spectral resolution or other errors are on the order of the difference in position of the band. Given the high R^2 values we have for our data (Tables 1–5, 7), we argue that the spectral bands that shift by the largest amounts over the Mg-Fe olivine solid solution (large Δ_{band}) would be useful for compositional determination, and may be as good a discriminator of olivine composition as fundamental band shifts. *Burns and Huggins* [1972] also recommend using spectral bands that "show an adequate frequency range between end member compositions" to reduce the errors in compositional estimates.

5.2. Flection Positions (and the Christiansen Frequency)

[46] The flection point of every Mg-Fe olivine spectrum measured occurs in the range of ~395 to 490 cm^{-1}, between bands 9 and 12 (Table 6), which is the area of the spectrum that generally divides the bands related to internal vibrations and the external vibrations. The flection point in each of our data sets (thermal emissivity, specular reflectivity, diffuse reflectivity pellet and powder, and attenuated total reflectivity) underwent the greatest displacement of *any* spectral feature in our Mg-Fe olivine suite (Figure 11 and Table 7). In the worst case (diffuse reflectivity powder data), the flection point moved 23% more than the greatest single band displacement for that technique. In the best case (attenuated total reflectivity powder data), the flection point moved 64% farther than the greatest single-band wave number displacement for that technique. On average, the flection point shift is 46% greater than the largest shift of the fundamental bands. We argue that this large flection point displacement (for all of the midinfrared spectral techniques presented in this paper) is a feature of any Mg-Fe olivine spectrum that could be exploited for determination of $Fo_{\#}$. Plus, the linear regression fits of the flection position data as they vary with composition were all better than the average fundamental band data in terms of both R^2 and 2σ (Tables 6 and 7), except for the attenuated total reflectivity data. The 2σ values for the flection points of all of the spectral techniques fell between 8.64 and 21.85, with the mean = 13.09. These values suggest that if one were to estimate olivine composition using the flection position, the predicted composition would fall within ±~13 mol % Fo for 95% of the cases. If the attenuated total reflectivity data were not included in the five-technique averages, then the flection point 2σ values would fall between 8.64 and 14.89, with the mean = 10.90.

[47] Our flection point displacements were all large ($\Delta_{flection}$ = 88–92 cm^{-1}; Table 7) compared with the change in fundamental band positions over the full range of $Fo_{\#}$ (Tables 1–5). *Hamilton* [2010] noted that the primary Christiansen frequency of the olivine data she studied also moved by a similar amount (Δ_{CF} = 87 cm^{-1} for emissivity data [2σ = 8.98]; also approximately that magnitude for graphed reflectivity data, but not specifically listed). This similar spectral dynamic range suggests that flection position and CF may both be good indicators of olivine composition (as well as fundamental band position).

[48] Preliminary application of the synthetic olivine flection position shift to the study of Mars Global Surveyor Thermal Emission Spectrometer (TES) data [*Christensen et al.*, 2001a] are promising, despite the lower spectral resolution of the TES data. After degrading the laboratory synthetic olivine spectra presented in this paper to TES resolution, the best TES instrument bands were identified that correlate to spectral bands 9 and 12 and the flection position in between. Using those identified instrument channels, an "olivine index" was defined and global olivine index maps were made for Mars that highlighted diverse olivine compositions over many different global regions [e.g., *Lane et al.*, 2009; *Lane and Goodrich*, 2010; M. D. Lane, unpublished data, 2011]. There are many caveats involved with "index" or any type of band parameter mapping using remote sensing or telescopic data of different targets (atmospheric removal, mineral mixtures, instrument noise, etc.); however, midinfrared index maps have been shown to be effective in identifying and mapping the geologic distribution of hematite on Mars using an emissivity maximum to define the index [*Christensen et al.*, 2000b, 2001b; *Glotch and Christensen*, 2005; *Glotch and Rogers*, 2007].

5.3. Band Width Changes

[49] The only band width-related data we studied were for the transparency band seen in the diffuse reflectivity spectra of powdered olivine at ~800 cm^{-1} (Figure 4). This band was visible only because of the fine-grained nature of the samples. We are unaware of any other study that has presented the determination of olivine composition on the basis of transparency band width. *Hofmeister and Pitman* [2007] published a figure relating olivine composition to bandwidth of the fundamental bands, but not to a transparency band. Our data support a linear relationship between transparency band width and composition (Figure 13), but data from *Hofmeister and Pitman* [2007] suggest a nonlinear relationship between fundamental band width and composition (although there is "considerable scatter" in their data). The usefulness of this transparency band/composition relationship may be fairly limited, because an "unknown" spectrum for comparison must also represent a fine-grained material and exhibit this olivine transparency band. None-

theless, the powdered olivine diffuse reflectivity spectra returned a strong linear relationship between transparency band width and mol % Fo composition (R^2 = 0.95; 2σ = 12.84). A complete study of transparency band width as it relates to variable particle size was not conducted in this work to isolate size effects from compositional effects; however, our particles are considered to be uniform in size because the samples were all synthesized and powdered in a uniform way [*Dyar et al.*, 2009]; therefore, this transparency band width trend (Figure 13) applies to particles <45 μm in diameter.

5.4. Use of More than One Band for Determining Composition

[50] The analyses of our multitechnique spectral data focused solely on single-parameter determinations of olivine composition (i.e., either shifting of the fundamental band position, shifting of the flection position, or width variation of the transparency band). All of these strategies (with the exception of a few bands) had high R^2 values and 2σ values that indicated that even one feature generally can provide an olivine composition to ±10–20 mol % Fo. If using a single band for olivine composition determination, certain bands are decidedly worse for $Fo_{\#}$ determination (e.g., bands 4 and 5, and other bands that are not traceable throughout the entire forsterite to fayalite series such as bands 3 (except in diffuse reflectivity powder data), 7, 10, 11, 13, and 14) and other bands are best for $Fo_{\#}$ determination (i.e., bands 9 and 12, and in some cases band 6).

[51] However, if more than one single parameter were used to estimate composition, the accuracy in determining $Fo_{\#}$ should improve [e.g., *Koeppen and Hamilton*, 2008; *Hamilton*, 2010]. For example, one could examine the fundamental band shift for more than one band, examine the shift for one band in conjunction with the CF shift, or examine the CF shift and the flection position shift. Moreover, if all of the parameters are examined, the best determination of $Fo_{\#}$ will occur. This multiple-parameter strategy is essentially what is employed when linear spectral (un) mixing [e.g., *Adams et al.*, 1986; *Ramsey*, 1996; *Ramsey and Christensen*, 1998] is used to identify the mineralogy in an unknown rock or meteorite (or mineral separate) spectrum. The researcher must determine when it is best to use these single- or multiple-parameter strategies and identify the errors associated with their study (be it a laboratory-based or remote sensing study).

6. Summary and Conclusions

[52] The main focus of this work is the analysis of pelletized synthetic, pure Mg-Fe olivine samples using thermal infrared emission, specular reflectance, and diffuse reflectance spectroscopic techniques, with additional analyses of powdered samples using diffuse reflectance and attenuated total reflectance spectroscopies. Given the challenging physical nature of these synthetic samples (i.e., very small quantities of pure powders and the small size of the resulting disc-shaped pellets (some of which broke into pieces) that are smaller than or at the spot size of the instruments, and the requirement of background removal for some data), the resulting midinfrared spectra are of good quality and provide very useful midinfrared data at fine $Fo_{\#}$ increments for this multitechnique study.

[53] The resulting synthetic olivine spectra are shown to exhibit similar behaviors among the various techniques of thermal emission, specular reflectance, and diffuse reflectance measurements of pellets (Figures 1–3 and 11) and the diffuse reflectance and attenuated total reflectance measurements of powders (Figures 4 and 5), in that the spectra from each technique generally follow similar trends as specified below. Sixteen distinct bands are identified in this binary Mg-Fe solid solution series, and 10 bands are traceable in each spectrum throughout the range of compositions. These 10 fundamental spectral features (Reststrahlen bands) are demonstrated to shift from higher frequencies (shorter wavelengths) associated with the Mg-rich olivines to lower frequencies (smaller wave numbers) associated with the Mg-poor olivines, as has been demonstrated before in the literature [e.g., *Tarte*, 1963; *Duke and Stephens*, 1964; *Burns and Huggins*, 1972; *Farmer*, 1974; *Jeanloz*, 1980; *Reynard*, 1991; *Hofmeister*, 1987, 1997; *Chopelas*, 1991; *Fabian et al.*, 2001; *Koike et al.*, 2003; *Kolesov and Geiger*, 2004; *Hofmeister and Pitman*, 2007; *Koeppen and Hamilton*, 2008; *Pitman et al.*, 2010; *Hamilton*, 2010]. Additionally, a flection position (i.e., a specific emissivity maximum/reflectance minimum that occurs between the internal and external vibrational modes in the ~395 to 490 cm^{-1} range) is exhibited in each pellet and powder spectrum for all spectral techniques, and is demonstrated in this study to shift from higher frequencies (for forsterite) to lower frequencies (for fayalite), similar to behavior of the fundamental bands, but by a larger amount (23–64% more than the largest Reststrahlen band shift). Also identified is a linear relationship between transparency band width and mol % Fo in diffuse reflectivity spectra of powdered olivine.

[54] Individually, these studied individual band parameters (fundamental band shift, flection position shift, transparency band width (and CF, as discussed in the text)) may be used to determine Mg-Fe olivine composition. We determined the following, according to the calculated 2σ values: (1) the *best* single fundamental band shift should predict the composition to ±~7–10 mol % Fo, but *typically*, most fundamental band position shifts would estimate the composition to ±10–20 mol % Fo; (2) the flection position should estimate the olivine composition to ±~11–13 mol % Fo; and (3) when applicable, the transparency band width compositional estimate should be correct to within ±~13 mol % Fo (as determined for the sample conditions presented).

[55] These band parameters, established for thermal emissivity, specular reflectivity, diffuse reflectivity, and attenuated total reflectivity spectra could be used for comparison with equivalent laboratory spectra or remote sensing/telescopic data to provide compositional estimates for olivine. In the pelletized sample and attenuated total reflectivity spectra, the fundamental bands are strong, and in fine-particulate diffuse reflectivity spectra they are weak, but the transparency band is strong; however, in *all* cases, the flection point is obvious and measureable, and shifts to a greater degree than any other band parameter studied here within the same data set. Hence, we argue that the shift in the position of the flection point (that lies between bands 9 and 12) should be considered, in addition to the traditional fundamental band positions, as a means of determining Mg-Fe olivine composition when using thermal emission, specular reflectance,

diffuse reflectance, or attenuated total reflectance spectroscopic data for the estimation of mol % Fo.

7. Future Work

[56] Because olivine is so prevalent in the solar system, spacecraft and telescopic data of various objects (e.g., asteroids, planetary surfaces, comet nuclei, and circumstellar disks), comparison of these olivine-rich data with a suite of laboratory-derived synthetic olivine spectra can help to identify the presence and composition of olivine. The attenuated total reflectivity data presented here would only be applicable in a situation where there is an in situ sample measurement. Thermal emission, specular reflectance, diffuse reflectance, and attenuated total reflectance spectroscopies all could be useful for nondestructive, chemical determination of an Mg-Fe olivine-bearing sample of unknown composition without damaging the sample. We have not explored the lower limits of how much olivine must be present in an unknown for our olivine spectra to be properly applied for olivine detection and compositional determination. These types of studies remain to be done.

[57] In this study we demonstrate the linear relationships of Mg-Fe olivine composition to fundamental band position, to flection position, and to transparency band width, and address the capabilities of a single parameter for determining olivine composition. In order to improve the olivine compositional assessment of an unknown spectrum, it should be better to apply more than one parameter for deciphering the composition of the olivine in the unknown spectrum. Fitting multiple fundamental bands or a combination of fundamental bands with flection position or transparency bandwidth should improve the determination of olivine presence and its composition. Initial application of our synthetic olivine spectra to some meteorite spectra and Martian remote sensing data has shown promise for identifying olivine composition by investigating as many spectral parameters as the data avail, even with the greater difficulties presented (other minerals present in the meteorites and typically lower signal to noise of the spacecraft data, fine-grained surface material, etc.), and application of our synthetic olivine spectra to other diverse data sets will help us further constrain the benefits of a single- versus multiple-parameter approach.

[58] **Acknowledgments.** Thanks are extended to Donald Lindsley at SUNY Stony Brook for synthesizing the olivine samples and to Phil Christensen at Arizona State University for the use of his thermal emission spectrometer facility. This work is supported by NASA's Mars Fundamental Research and Mars Odyssey Programs and is PSI contribution 507. Detailed reviews by Vicky Hamilton and an anonymous reviewer are greatly appreciated and resulted in an improved manuscript.

References

Adams, J. B., M. O. Smith, and P. E. Johnson (1986), Spectral mixture modeling: A new analysis of rock and soil types at the Viking Lander 1 site, *J. Geophys. Res.*, *91*, 8098–8112, doi:10.1029/JB091iB08p08098.

Aronson, J. R., and A. G. Emslie (1973), Spectral reflectance and emittance of particulate materials, 2, Applications and results, *Appl. Opt.*, *12*, 2573–2584, doi:10.1364/AO.12.002573.

Aronson, J. R., A. G. Emslie, and H. G. McLinden (1966), Infrared spectra from particulate surfaces, *Science*, *152*, 345–346, doi:10.1126/science.152.3720.345-a.

Bandfield, J. L., and A. D. Rogers (2008), Olivine dissolution by acidic fluids in Argyre Planitia, Mars: Evidence for a widespread process?, *Geology*, *36*, 579–582, doi:10.1130/G24724A.1.

Bowey, J. E., C. Lee, C. Tucker, A. M. Hoefmeister, P. A. R. Ade, and M. J. Barlow (2001), Temperature effects on the 15–85 μm spectra of olivines and pyroxenes, *Mon. Not. R. Astron. Soc.*, *325*, 886–896, doi:10.1046/j.1365-8711.2001.04523.x.

Burns, R. G. (1970), Crystal field spectra and evidence of cation ordering in olivine minerals, *Am. Mineral.*, *55*, 1608–1632.

Burns, R. G., and F. E. Huggins (1972), Cation determinative curves from Mg-Fe-Mn olivines from vibrational spectra, *Am. Mineral.*, *57*, 967–985.

Chemtob, S. M., T. G. Glotch, and G. R. Rossman (2010), ATR-IR spectroscopy for in situ mineral analysis on planetary surfaces: Steps toward a forward model, *Lunar Planet. Sci., XLI*, Abstract 2198.

Chopelas, A. (1991), Single crystal Raman spectra of forsterite, fayalite, and monticellite, *Am. Mineral.*, *76*, 1101–1109.

Christensen, P. R., J. L. Bandfield, M. D. Smith, V. E. Hamilton, and R. N. Clark (2000a), Identification of a basaltic component on the Martian surface from Thermal Emission Spectrometer data, *J. Geophys. Res.*, *105*, 9609–9621, doi:10.1029/1999JE001127.

Christensen, P. R., et al. (2000b), Detection of crystalline hematite mineralization on Mars by the Thermal Emission Spectrometer: Evidence for near-surface water, *J. Geophys. Res.*, *105*, 9623–9642, doi:10.1029/1999JE001093.

Christensen, P. R., et al. (2001a), Mars Global Surveyor Thermal Emission Spectrometer experiment: Investigation description and surface science results, *J. Geophys. Res.*, *106*, 23,823–23,871, doi:10.1029/2000JE001370.

Christensen, P. R., R. V. Morris, M. D. Lane, J. L. Bandfield, and M. C. Malin (2001b), Global mapping of Martian hematite mineral deposits: Remnants of water-driven processes on early Mars, *J. Geophys. Res.*, *106*, 23,873–23,885, doi:10.1029/2000JE001415.

Clark, R. N., G. A. Swayze, R. A. Wise, K. E. Livo, T. M. Hoefen, R. F. Kokaly, and S. J. Sutley (2007) USGS digital spectral library splib06a, *Digital Data Ser. 231*, U.S. Geol. Surv., Reston, Va. (Available at http://speclab.cr.usgs.gov/spectral.lib06.)

Conel, J. E. (1969), Infrared emissivities of silicates: Experimental results and a cloudy atmosphere model of spectral emission from condensed particulate mediums, *J. Geophys. Res.*, *74*, 1614–1634, doi:10.1029/JB074i006p01614.

Cooper, B. L., J. W. Salisbury, R. M. Killen, and A. E. Potter (2002), Mid-infrared spectral features of rocks and their powders, *J. Geophys. Res.*, *107*(E4), 5017, doi:10.1029/2000JE001462.

Cruikshank, D. P., and W. K. Hartmann (1984), The meteorite-asteroid connection: Two olivine-rich asteroids, *Science*, *223*, 281–283, doi:10.1126/science.223.4633.281.

Duke, D. A., and J. D. Stephens (1964), Infrared investigation of the olivine group minerals, *Am. Mineral.*, *49*, 1388–1406.

Dyar, M. D., et al. (2009), Spectroscopic characteristics of synthetic olivine: An integrated multi-wavelength and multi-technique approach, *Am. Mineral.*, *94*, 883–898, doi:10.2138/am.2009.3115.

Dyar, M. D., et al. (2011), Spectroscopy of Yamato 984028, *Polar Res.*, *4*, 530–549, doi:10.1016/j.polar.2010.06.001.

Edwards, C. S., P. R. Christensen, and V. E. Hamilton (2008), Evidence for extensive olivine-rich basalt bedrock outcrops in Ganges and Eos chasmas, Mars, *J. Geophys. Res.*, *113*, E11003, doi:10.1029/2008JE003091.

Fabian, D., T. Henning, C. Jäger, H. Mutschke, J. Dorschner, and O. Wehrhan (2001), Steps toward interstellar silicate mineralogy: VI. Dependence of crystalline olivine IR spectra on iron content and particle shape, *Astron. Astrophys.*, *378*, 228–238, doi:10.1051/0004-6361:20011196.

Farmer, V. C. (1974), Orthosilicates, pyrosilicates, and other finite-chain silicates, in *The Infrared Spectra of Minerals*, edited by V. C. Farmer, pp. 285–303, Mineral. Soc., London.

Gaffey, M. J., J. F. Bell, R. H. Brown, T. H. Burbine, J. L. Piatek, K. L. Reed, and D. A. Chaky (1993a), Mineralogical variation within the S-type asteroid class, *Icarus*, *106*, 573–602, doi:10.1006/icar.1993.1194.

Gaffey, S. J., L. A. McFadden, D. Nash, and C. M. Pieters (1993b), Ultraviolet, visible, and near-infrared reflectance spectroscopy: Laboratory spectra of geologic materials, in *Remote Geochemical Analysis: Elemental and Mineralogical Composition*, edited by C. M. Pieters and P. J. Englert, pp. 43–78, Cambridge Univ. Press, Cambridge, U. K.

Glotch, T. D., and P. R. Christensen (2005), Geologic and mineralogic mapping of Aram Chaos: Evidence for a water-rich history, *J. Geophys. Res.*, *110*, E09006, doi:10.1029/2004JE002389.

Glotch, T. D., and A. D. Rogers (2007), Evidence for aqueous deposition of hematite- and sulfate-rich light-toned layered deposits in Aureum and Iani Chaos, Mars, *J. Geophys. Res.*, *112*, E06001, doi:10.1029/2006JE002863.

Glotch, T. D., R. V. Morris, P. R. Christensen, and T. G. Sharp (2004), Effect of precursor mineralogy on the thermal infrared emission spectra

of hematite: Application to Martian hematite mineralization, *J. Geophys. Res.*, *109*, E07003, doi:10.1029/2003JE002224.

Glotch, T. D., G. R. Rossman, and O. Aharonson (2007), Mid-infrared (5–100 μm) reflectance spectra and optical constants of ten phyllosilicate minerals, *Icarus*, *192*, 604–622, doi:10.1016/j.icarus.2007.07.002.

Hamilton, V. E. (2010), Thermal infrared (vibrational) spectroscopy of Mg-Fe olivines: A review and applications to determining the composition of planetary surfaces, *Chem. Erde*, *70*, 7–33, doi:10.1016/j.chemer.2009.12.005.

Hamilton, V. E., and P. R. Christensen (2005), Evidence for extensive, olivine-rich bedrock on Mars, *Geology*, *33*, 433–436, doi:10.1130/G21258.1.

Hamilton, V. E., and M. E. Minitti (2003), Are oxidized shergottite-like basalts an alternative to "andesite" on Mars?, *Geophys. Res. Lett.*, *30*(18), 1915, doi:10.1029/2003GL017839.

Hapke, B. (1993), *Theory of Reflectance and Emittance Spectroscopy*, 445 pp., Cambridge Univ. Press, New York, doi:10.1017/CBO9780511524998.

Harrick, N. J. (1967), *Internal Reflection Spectroscopy*, 327 pp., Interscience, New York.

Hoefen, T. M., R. N. Clark, J. L. Bandfield, M. D. Smith, J. C. Pearl, and P. R. Christensen (2003), Discovery of olivine in the Nili Fossae region of Mars, *Science*, *302*, 627–630, doi:10.1126/science.1089647.

Hofmeister, A. M. (1987), Single-crystal absorption and reflection infrared spectroscopy of forsterite and fayalite, *Phys. Chem. Miner.*, *14*, 499–513, doi:10.1007/BF00308285.

Hofmeister, A. M. (1997), Infrared reflectance spectra of fayalite, and adsorption data from assorted olivines, including pressure and isotope effects, *Phys. Chem. Miner.*, *24*, 535–546, doi:10.1007/s002690050069.

Hofmeister, A. M., and H. Mao (2002), Redefinition of the mode Grüneisen parameter for polyatomic substances and thermodynamic implications, *Proc. Natl. Acad. Sci. U. S. A.*, *99*(2), 559–564, doi:10.1073/pnas.241631698.

Hofmeister, A. M., and K. M. Pitman (2007), Evidence for kinks in structural and thermodynamic properties across the forsterite-fayalite binary from thin-film IR absorption spectra, *Phys. Chem. Miner.*, *34*, 319–333, doi:10.1007/s00269-007-0150-1.

Huggins, F. E. (1973), Cation order in olivines: Evidence from vibrational spectra, *Chem. Geol.*, *11*, 99–108, doi:10.1016/0009-2541(73)90046-6.

Hunt, G. R., and L. M. Logan (1972), Variation of single particle mid-infrared emission spectrum with particle size, *Appl. Opt.*, *11*, 142–147, doi:10.1364/AO.11.000142.

Hunt, G. R., and R. K. Vincent (1968), The behavior of spectral features in the infrared emission from particulate surfaces of various grain sizes, *J. Geophys. Res.*, *73*, 6039–6046, doi:10.1029/JB073i018p06039.

Iishi, K. (1978), Lattice dynamics of forsterite, *Am. Mineral.*, *63*, 1198–1208.

Jäger, C., F. J. Molster, J. Dorschner, T. Henning, H. Mutschke, and L. B. F. M. Waters (1998), Steps toward interstellar silicate mineralogy: IV. The crystalline revolution, *Astron. Astrophys.*, *339*, 904–916.

Jeanloz, R. (1980), Infrared spectra of olivine polymorphs: α, β phase and spinel, *Phys. Chem. Miner.*, *5*, 327–341, doi:10.1007/BF00307542.

Koeppen, W. C., and V. E. Hamilton (2008), Global distribution, composition, and abundance of olivine on the surface of Mars from thermal infrared data, *J. Geophys. Res.*, *113*, E05001, doi:10.1029/2007JE002984.

Koike, C., H. Chihara, A. Tsuchiyama, H. Suto, H. Sogawa, and H. Okuda (2003), Compositional dependence of infrared absorption spectra of crystalline silicate, *Astron. Astrophys.*, *399*, 1101–1107, doi:10.1051/0004-6361:20021831.

Kolesov, B. A., and C. A. Geiger (2004), A Raman spectroscopic study of Fe-Mg olivines, *Phys. Chem. Miner.*, *31*, 142–154, doi:10.1007/s00269-003-0370-y.

Lane, M. D. (1999), Mid-infrared optical constants of calcite and their relationship to particle size effects in thermal emission spectra of granular calcite, *J. Geophys. Res.*, *104*, 14,099–14,108, doi:10.1029/1999JE900025.

Lane, M. D., and P. R. Christensen (1998), Thermal infrared emission spectroscopy of salt minerals predicted for Mars, *Icarus*, *135*, 528–536, doi:10.1006/icar.1998.5998.

Lane, M. D., and C. A. Goodrich (2010), High-magnesian olivine in the Argyre rim: Derived from a primitive magma?, *Lunar Planet. Sci., XLI*, Abstract 2094.

Lane, M. D., T. D. Glotch, M. D. Dyar, J. L. Bishop, C. M. Pieters, R. Klima, T. Hiroi, and J. M. Sunshine (2009), Thermal infrared spectroscopy of a synthetic olivine series (forsterite-fayalite) and interpretation of the Nili Fossae, Syrtis Major, and Isidis regions of Mars, *Lunar Planet. Sci., XL*, Abstract 2469.

Lehmann, H., H. Dutz, and M. Koltermann (1961), Ultrarotspektroskopische Untersuchungen zur Mischkirstallreihe Forsterit-Fayalit, *Ber. Dtsch. Keram. Ges.*, *38*, 512–514.

Lucey, P. G., K. Keil, and R. Whitely (1998), The influence of temperature on the spectra of the A-asteroids and implications for their silicate chemistry, *J. Geophys. Res.*, *103*, 5865–5871, doi:10.1029/97JE03691.

Lyon, R. J. P. (1964), Evaluation of infrared spectrophotometry for compositional analysis of lunar and planetary soils, II, Rough and powdered surfaces, *NASA Conf. Rep., CR-100*.

McSween, H. Y., Jr., et al. (2006), Characterization and petrologic interpretation of olivine-rich basalts at Gusev Crater, Mars, *J. Geophys. Res.*, *111*, E02S10, doi:10.1029/2005JE002477.

Moersch, J. E. (1992) Modeling particle size effects on the emissivity spectra of minerals in the thermal infrared, M.S. thesis, Ariz. State Univ., Tempe.

Moersch, J. E., and P. R. Christensen (1995), Thermal emission from particulate surfaces: A comparison of scattering models with measured spectra, *J. Geophys. Res.*, *100*, 7465–7477, doi:10.1029/94JE03330.

Mustard, J. F., and J. E. Hays (1997), Effects of hyperfine particles on reflectance spectra from 0.3 to 25 μm, *Icarus*, *125*, 145–163, doi:10.1006/icar.1996.5583.

Nash, D. B., and J. W. Salisbury (1991), Infrared reflectance spectra (2.2–15 μm) of plagioclase feldspars, *Geophys. Res. Lett.*, *18*(6), 1151–1154, doi:10.1029/91GL01008.

Nicodemus, F. E. (1965), Directional reflectance and emissivity of an opaque surface, *Appl. Opt.*, *4*(7), 767–773, doi:10.1364/AO.4.000767.

Pieters, C. M. (1982), Copericus crater central peak: Lunar mountain of unique composition, *Science*, *215*, 59–61, doi:10.1126/science.215.4528.59.

Pieters, C. M., and T. Hiroi (2004) RELAB (Reflectance Experiment Laboratory): A NASA multiuser spectroscopy facility, *Lunar Planet. Sci. [CD-ROM], XXXV*, Abstract 1720.

Piriou, B., and P. McMillan (1983), The high-frequency vibrational spectra of vitreous and crystalline orthosilicates, *Am. Mineral.*, *68*, 426–443.

Pitman, K. M., C. R. Dijkstra, A. M. Hofmeister, and A. K. Speck (2010), Infrared laboratory absorbance spectra of olivine: Using classical dispersion analysis to extract peak parameters, *Mon. Not. R. Astron. Soc.*, *406*, 460–481, doi:10.1111/j.1365-2966.2010.16669.x.

Poulet, F., C. Gomez, J.-P. Bibring, Y. Langevin, B. Gondet, P. Pinet, G. Belluci, and J. Mustard (2007), Martian surface mineralogy from Obervatoire pour la Mineralogie, l'Eau, les Glaces et l'Activite on board the Mars Express spacecraft (OMEGA/MEx): Global mineral maps, *J. Geophys. Res.*, *112*, E08S02, doi:10.1029/2006JE002840.

Ramsey, M. S. (1996) Quantitative analysis of geological surfaces: A deconvolution algorithm for midinfrared remote sensing data, Ph.D. dissertation, 276 pp., Ariz. State Univ., Tempe.

Ramsey, M. S., and P. R. Christensen (1998), Mineral abundance determination: Quantitative deconvolution of thermal emission spectra, *J. Geophys. Res.*, *103*, 577–596, doi:10.1029/97JB02784.

Reynard, B. (1991), Single-crystal infrared reflectivity of pure Mg_2SiO_4 forsterite and $(Mg_{0.86}, Fe_{0.14})_2SiO_2$ olivine, *Phys. Chem. Miner.*, *18*, 19–25, doi:10.1007/BF00199039.

Rogers, A. D., and P. R. Christensen (2007), Surface mineralogy of Martian low-albedo regions from MGS-TES data: Implications for upper crustal evolution and surface alteration, *J. Geophys. Res.*, *112*, E01003, doi:10.1029/2006JE002727.

Roush, T., J. Pollack, and J. Orenberg (1991), Derivation of midinfrared (5–25 μm) optical constants of some silicates and palagonite, *Icarus*, *94*, 191–208, doi:10.1016/0019-1035(91)90150-R.

Ruff, S. W., P. R. Christensen, P. W. Barbera, and D. L. Anderson (1997), Quantitative thermal emission spectroscopy of minerals: A laboratory technique for measurement and calibration, *J. Geophys. Res.*, *102*, 14,899–14,913, doi:10.1029/97JB00593.

Ruff, S. W., P. R. Christensen, D. L. Blaney, W. H. Farrand, J. R. Johnson, J. R. Michalski, J. E. Moersch, S. P. Wright, and S. P. Squyres (2006), The rocks of Gusev Crater as viewed by the Mini-TES instrument, *J. Geophys. Res.*, *111*, E12S18, doi:10.1029/2006JE002747.

Runciman, W. A., D. Sengupta, and J. T. Gourley (1973), The polarized spectra of iron in silicates, II, olivine, *Am. Mineral.*, *58*, 451–456.

Salisbury, J. W., and J. W. Eastes (1985), The effect of particle size and porosity on spectral contrast in the mid-infrared, *Icarus*, *64*, 586–588, doi:10.1016/0019-1035(85)90078-8.

Salisbury, J. W., and A. E. Wald (1992), The role of volume scattering in reducing spectral contrast in spectra of powdered minerals, *Icarus*, *96*, 121–128, doi:10.1016/0019-1035(92)90009-V.

Salisbury, J. W., B. Hapke, and J. W. Eastes (1987), Usefulness of weak bands in midinfrared remote sensing of particulate planetary surfaces, *J. Geophys. Res.*, *92*, 702–710, doi:10.1029/JB092iB01p00702.

Salisbury, J. W., D. M. D'Aria, and E. Jarosewich (1991a), Midinfrared (2.5–13.5 μm) reflectance spectra of powdered stony meteorites, *Icarus*, *92*, 280–297, doi:10.1016/0019-1035(91)90052-U.

Salisbury, J. W., L. S. Walter, N. Vergo, and D. M. D'Aria (1991b), *Infrared (2.1–25 μm) Spectra of Minerals*, Johns Hopkins Univ. Press, Baltimore, Md.

Servoin, J. L., and B. Piriou (1973), Infrared reflectivity and Raman scattering of Mg2SiO4 single crystal, *Phys. Status Solidi B*, *55*, 677–686, doi:10.1002/pssb.2220550224.

Sogawa, H., C. Koike, H. Chihara, H. Suto, S. Tachibana, A. Tsuchiyama, and T. Kozasa (2006), Infrared reflection spectra of forsterite crystal, *Astron. Astrophys.*, *451*, 357–361, doi:10.1051/0004-6361:20041538.

Sunshine, J. M., J. Schelte, C. M. Corrigan, T. J. McCoy, and T. H. Burbine (2007), Olivine-dominated asteroids and meteorites: Distinguishing nebular and igneous histories, *Meteorit. Planet. Sci.*, *42*, 155–170, doi:10.1111/j.1945-5100.2007.tb00224.x.

Tarantino, S. C., M. A. Carpenter, and M. C. Domeneghetti (2003), Strain and local heterogeneity in the forsterite-fayalite solid solution, *Phys. Chem. Miner.*, *30*, 495–502, doi:10.1007/s00269-003-0357-8.

Tarte, P. (1963), Etude infra-rouge des orthosilicates et des orthogermanates, *Spectrochim. Acta*, *19*, 25–47, doi:10.1016/0371-1951(63)80092-2.

Vincent, R. K., and G. R. Hunt (1968), Infrared reflectance from mat surfaces, *Appl. Opt.*, *7*, 53–58, doi:10.1364/AO.7.000053.

Wagner, C. (2000) Thermal emission spectroscopy of laboratory regoliths, in *Thermal Emission Spectroscopy and Analysis of Dust, Disks, and Regoliths*, *Conf. Ser.*, vol. 196, edited by M. L. Sitko, A. L. Sprague, and D. K. Lynch, pp. 233–247, Astron. Soc. of the Pac., San Francisco, Calif.

Wald, A. E. (1999), Modeling thermal infrared (2–14 microns) reflectance spectra of frost and snow, *J. Geophys. Res.*, *94*, 24,241–24,250, doi:10.1029/94JB01560.

Wald, A. E., and J. W. Salisbury (1995), Thermal infrared directional emissivity of powdered quartz, *J. Geophys. Res.*, *100*, 24,665–24,675, doi:10.1029/95JB02400.

Wenrich, M. L., and P. R. Christensen (1996), Optical constants of minerals derived from emission spectroscopy: Application to quartz, *J. Geophys. Res.*, *101*, 15,921–15,931, doi:10.1029/96JB01153.

Young, T. R., and B. D. Rothrock (1963), Theory of frustrated total reflection involving metallic surfaces, *J. Res. Natl. Bur. Stand. A*, *67*, 115–125.

J. L. Bishop, SETI Institute, 515 N. Whisman Rd., Mountain View, CA 94043, USA.

M. D. Dyar, Department of Astronomy and Geology, Mount Holyoke College, 50 College St., South Hadley, MA 01075, USA.

T. D. Glotch, Department of Geosciences, 250 Earth and Space Sciences Bl, State University of New York at Stony Brook, Stony Brook, NY 11794, USA.

T. Hiroi and C. M. Pieters, Department of Geological Sciences, PO Box 1846, Brown University, Providence, RI 02912, USA.

R. Klima, Space Department, Johns Hopkins University Applied Physics Laboratory, 11100 Johns Hopkins Rd., Laurel, MD 20723, USA.

M. D. Lane, Planetary Science Institute, 1700 E. Fort Lowell Rd., Ste. 106, Tucson, AZ 85719, USA. (lane@psi.edu)

J. Sunshine, Department of Astronomy, University of Maryland, Computer and Space Sciences Bldg., College Park, MD 20742, USA.